UNIVERSIDADE D
COIMBRA

Beatriz Barata Fazendeiro

DECIPHERING THE FUNCTIONS OF NDR KINASES AS NOVEL PLAYERS IN THE REGULATION OF MICROGLIA

Dissertação no âmbito do Mestrado em Biotecnologia Farmacêutica orientada pela Doutora Hélène Marie Léger e pelo Doutor Luís Fernando Morgado Pereira de Almeida e apresentada Faculdade de Farmácia da Universidade de Coimbra.

Setembro 2023

UNIVERSIDADE D
COIMBRA

DECIPHERING THE FUNCTIONS OF NDR KINASES AS NOVEL PLAYERS IN THE REGULATION OF MICROGLIA

Beatriz Barata Fazendeiro

The experimental work described in the present thesis was performed at Retinal Dysfunction and Neuroinflammation Lab, Coimbra Institute for Clinical and Biomedical Research (iCBR), Faculty of Medicine, University of Coimbra.

This work was supported by the Foundation for Science and Technology (FCT), Portugal (2022.06170.PTDC) and Strategic Project (PEst UID/NEU/04539/2013UIDB/04539/2020 and UIDP/04539/2020).

1 2 9 0 UNIVERSIDADE D COIMBRA

iCBR

fct Fundação para a Ciência e a Tecnologia

QREN QUADRO DE REFERÊNCIA ESTRATÉGICO NACIONAL PORTUGAL 2007.2013

"The future belongs to those who believe in the beauty of their dreams."

Eleanor Roosevelt

Agradecimentos:

Em primeiro lugar quero agradecer à minha orientadora Doutora Hélène Léger por me ter dado a oportunidade de desenvolver o meu projeto de mestrado com ela e por ter acreditado em mim e no meu trabalho! Muito obrigada por toda a disponibilidade, calma e paciência ao longo deste ano!

Em segundo lugar gostaria de agradecer ao Doutor Luís Pereira de Almeida por ter aceitado fazer parte deste meu percurso, como meu co-orientador.

Agradecer também ao Doutor Paulo Santos, que apesar de nenhuma obrigação, teve um papel fundamental na minha orientação. Obrigada por todos os concelhos científicos, discussão de resultados e apoio neste percurso!

Ao Doutor Francisco Ambrósio, obrigada por me ter dado a oportunidade de fazer parte do seu grupo! Um obrigada também a todos os membros do grupo que, de alguma forma, me ajudaram ao longo destes meses, em especial a todas as minhas colegas de mestrado: Cristiana, Ângela, Jéssica e Rita.

À Doutora Filipa Baptista, obrigada por me ter acolhido no seu gabinete e por toda a disponibilidade demonstrada todas as vezes em que precisei de ajuda!

Um agradecimento especial à Doutora Lavínia Romera que me ensinou tudo o que eu sei sobre cultura celular, que me deu ritmo para fazer múltiplos ensaios ao mesmo tempo, que esteve sempre disposta a ajudar-me em tudo o que eu precisei e, por além de ter sido uma extraordinária orientadora, se ter tornado uma amiga!

Inês, obrigada por teres estado sempre lá, obrigada por me apresentares a todas as pessoas quando cai do nada neste laboratório, obrigada por estares sempre pronta para procrastinar comigo e falar de tudo e de nada, obrigada por lidares com o meu pior mood (que nunca foi pior que o teu!), obrigada por teres sido a melhor parceira (e amiga) de gabinete e laboratório e obrigada por toda a cumplicidade! Um obrigada não chega, nem nunca vai chegar! Gosto de ti com o meu coração <3

Albertine, um pequeno anjo que me caiu do céu e que, mais que ninguém, me ajudou na altura critica que foram os últimos dois meses de laboratório! Obrigada, sem ti não sei como é que teria lidado com as 240 lamelas e as 600 imagens para contar!

Quero também agradecer às pessoas do terceiro piso por terem elevado este ano a um outro nível! Ana Olívia obrigada por teres sempre uma vida muito preenchida e cheia de acontecimentos que nos permitem que nunca nos falte tema de conversa. Eliane, obrigada por ser a minha Gossip Girl e por me permitires ter tempos de procrastinação cada vez que precisavas de anticorpos. Alexandre, obrigada por todas as horas de almoço de discussão crítica de resultados (que nunca vão estar certos), de estatística (que eu juro que tentei entender) e por veres os mesmos programas que eu!

Por fim, aos meus pais, obrigada por todo o apoio, sem eles provavelmente não estaria onde estou hoje! Ao Fernando que esteve sempre lá para mim e à minha irmã por ter escrito (copy/paste) as abreviaturas desta tese!

Table of contents

List of Tables

List of Figures

Abbreviations

ARVO – Association for Research in Vision and Ophthalmology

BCA – Bicinchoninic acid

bp – Base pair

BSA – Bovine Serum Albumin

Cas – CRISPR associated

cDNA – Complementary DNA

CRISPR – Clustered regularly interspaced short palindromic repeat

crRNA – CRISPR RNA

CT – Control

DME – Diabetic macular edema

DMEM – Dulbecco's Modified Eagle Medium

DR – Diabetic retinopathy

DSB – Double-strand break

FBS – Fetal Bovine Serum

GCL – Ganglion cell layer

gRNA – Guide RNA

HDR – Homology-directed repair

HG – High glucose

ICC – Immunocytochemistry

IHC – Immunohistochemistry

IL – Interleukins

ILM – Internal limiting membrane

INL – Inner nuclear layer

IPL – Inner plexiform layer

IS – Inner segments of the photoreceptors

KO - Knockout

LATS – Large tumor suppressor

LPS – Lipopolysaccharide

M – Mannitol

MFI – Mean Fluorescence Intensity

MOB1 – Mps1-one binder

mqH2O – Milli-Q Water

MST – Mammalian STE20-like kinase

NDR – Nuclear Dbf2-related

NF-kB – Nuclear factor kappa B

NFL – Nerve fiber layer

NG – Normal glucose

NHEJ – Non-homologous end joining

NPRP – Non-proliferative diabetic retinopathy

NTR – N-terminal regulatory

NUC – Nuclease lobe

OLM – Outer limiting membrane

ONL – Outer nuclear layer

OPL – Outer plexiform layer

PAM – Protospacer adjacent motif

PBS – Phosphate-buffered saline

PDR – Proliferative diabetic retinopathy

Pen/Strep – Penicillin-Streptomycin

PFA – Paraformaldehyde

PI – Protospacer Adjacent Motif interacting

PL – Photoreceptor layer

PVDF – Polyvinylidene difluoride

qRT-PCR – Quantitative polymerase chain reaction

REC – Recognition lobe

RGCs – Retinal ganglion cells

ROS – Oxygen reactive species

RPE – Retinal pigment epithelium

RPMI – Roswell Park Memorial Institute

RT – Room temperature

SDS – Sodium dodecyl sulfate

sgRNA – Single-guide RNA

STK38 – Serine-threonine kinase 38

STK38L – Serine-threonine kinase 38 like

STZ – Streptozotocin

TAZ – WW Domain Containing Transcription Regulator1

TBS-T – Tris-buffered saline - tween 20

TNF-α – Tumor necrosis factor-alpha

tracrRNA – Trans-activating CRISPR RNA

WB – Western Blot

WT – Wild-type

YAP – Yes-associated protein

Abstract

Diabetic retinopathy is a severe complication of diabetes and a leading cause of visual impairment worldwide, predominantly affecting the working-age population. It is well established that chronic hyperglycemia plays a critical role in the pathogenesis of diabetic retinopathy, triggering an array of cellular responses within the retina. One of the key players involved in the retinal response against stress, such as chronic hyperglycemia, is microglia. Microglia are a type of cell that becomes activated in response to various pathological stimuli and can exert both neuroprotective and neurodegenerative effects. The NDR (Nuclear Dbf2-Related) kinases have emerged as crucial regulators of cell growth, survival, and migration in numerous biological contexts. Recent studies have implicated NDR kinases in neuroinflammation and neurodegenerative diseases, pointing to their potential involvement in the pathophysiology of diabetic retinopathy. However, the precise role of NDR kinases in the context of retinal microglial responses and hyperglycemic environments remains largely unexplored.

To address this gap, our study sought to investigate the effects of high glucose (HG) exposure on BV-2 microglial cells, with a specific focus on the role of NDR kinases in this process. BV-2 cells were chosen as an established *in vitro* model to study microglial responses, and by subjecting them to HG exposure, we aimed to mimic the hyperglycemic environment that occurs in diabetes. The cells were incubated with HG for different timepoints: 4h HG incubation (4h assay), 7h HG incubation (7h assay), two times 4h HG incubations with a 4h incubation break in between with normal glucose (12h assay) and then different assays were performed to address the main question. Additionally, we conducted a CRISPR-Cas9 lipofectamine transfection to induce a knockout of Ndr2 in BV-2 cells in order to understand the role of NDR2 kinase in microglial cells in the context of diabetes. Ultimately, an STZ-induced diabetic mouse model was used to evaluate the differences in retinal Ndr2 expression when compared to a non-diabetic animal.

Our findings highlight that NDR kinases are expressed in BV-2 microglial cells and that expression is impacted by exposure to acute levels of high glucose. Protein levels of NDR1/2 exhibited a reduction in BV-2 cells subjected to the 7h assay, yet they exhibited an increase when exposed to the 12h assay. The same pattern was observed for Ndr2 mRNA expression, suggesting that during the 4h break between HG exposures, the cells might activate compensatory mechanisms to mitigate the adverse effects of HG-induced stress. Conversely, such mechanisms might be inhibited during extended HG exposure periods (7h). Furthermore, our study demonstrates that Ndr2 downregulation influences phagocytosis, a

main function of microglial cells. Moreover, we confirmed the influence of the glycemic environment on the phagocytic activity of the microglial cells even in short-term exposures. For WT BV-2 cells, an increase was observed in the 4h assay, while in the 12h assay, phagocytic efficacy decreased. Nevertheless, the phagocytic activity of Ndr2 downregulated BV-2 cells was inherently less responsive to changes in glucose concentrations. This outcome can be a result of Ndr2 downregulation, but additional experiments are necessary given the potential influence of alternate signaling pathways on phagocytosis regulation. We also observed that HG exposure and Ndr2 downregulation lead to the expression of TNF-α and IL-17a, suggesting that NDR2 kinase is involved in the immune response mediated by microglial cells. Lastly, NDR2 expression in STZ-induced diabetic mice was observed in the inner plexiform layer, whereas in non-diabetic mice, the expression is in all layers of the retina, from the outer nuclear layer to the inner plexiform layer, suggesting that NDR kinases may have a role in modulating synaptic function and, consequently, the processing of visual information.

In conclusion, this study reveals that NDR2 might play an important role in diabetic retinopathy, affecting microglial cells and contributing to the retinal changes observed in diabetic patients. It also underscores the importance of further research to unravel the intricate connections between NDR kinases and microglial responses. Ultimately, deciphering these molecular mechanisms may pave the way for novel genetic testing or therapeutic strategies aimed at mitigating the effects of diabetic retinopathy and improving visual outcomes for affected individuals.

Keywords: Nuclear Dbf2-related (NDR) kinases, Microglia, Retina, High-glucose, Diabetic Retinopathy.

Resumo

A retinopatia diabética é uma complicação grave da diabetes e uma das principais causas de deficiência visual em todo o mundo. Vários estudos reportam que a hiperglicemia crónica desempenha um papel fundamental no desenvolvimento da retinopatia diabética e desencadeia vários processos celulares na retina em resposta a stress, como por exemplo elevados níveis de glucose. As células da microglia são um tipo de células que são ativadas em resposta a vários estímulos patológicos e que tanto podem exercer efeitos neuroprotetores como neurodegenerativos. Estas células são consideradas os principais mediadores na resposta da retina a condições de stress. As cinases NDR (Nuclear Dbf2-Related) têm surgido como reguladores cruciais do crescimento, sobrevivência e migração celular em vários contextos biológicos. Estudos recentes indicam que as cinases NDR estão envolvidas em processos de neuroinflamação e em doenças neurodegenerativas, o que reforça o seu potencial envolvimento na fisiopatologia da retinopatia diabética. No entanto, o papel exato destas cinases na resposta da microglia a condições de hiperglicemia permanece bastante inexplorado.

Para colmatar esta lacuna, o nosso estudo tem por base a investigação dos efeitos da exposição a níveis elevados de glucose (HG) nas células da microglia e o papel das cinases NDR ao longo desse processo. A linha celular BV-2 foi escolhida como um modelo *in vitro* para estudar as respostas da microglia e, ao submetê-las à exposição a elevados níveis de glucose, pretendemos reproduzir o ambiente hiperglicémico característico da diabetes. Para isso as células foram incubadas com HG durante diferentes períodos de tempo: 4h de incubação com HG (ensaio de 4h), 7h de incubação com HG (ensaio de 7h), duas incubações de 4h com HG com um intervalo de 4h de exposição, entre as mesmas, a níveis normais de glucose (ensaio de 12h). De seguida, foram efetuados diferentes ensaios de modo a responder à principal questão deste estudo. Além disso, utilizámos a técnica CRISPR-Cas9 para induzir um knockout do gene Ndr2 em células BV-2, com o intuito de compreender a função da cinase NDR2 em células da microglia e num contexto de diabetes. Por fim, utilizamos um modelo de murganho diabético, induzido por STZ, para avaliar as diferenças na expressão de Ndr2 na retina quando comparado com um animal não diabético.

Os nossos resultados indicam que, de facto, as cinases NDR são expressas em células BV-2 e que essa expressão é afetada pela exposição aguda a elevados níveis de glucose. Os níveis de expressão das proteínas NDR1/2 apresentaram uma redução nas células BV-2 submetidas ao ensaio de 7 horas, mas, por outro lado, foi observado um aumento de expressão quando as células foram submetidas ao ensaio de 12 horas. O mesmo padrão foi observado para a

expressão de mRNA de Ndr2, o que sugere que, durante o intervalo de 4 horas entre as exposições a elevados níveis de glucose, as células podem ativar mecanismos de compensação para atenuar os efeitos adversos provocados pela glucose. No entanto, esses mecanismos podem ser inibidos durante períodos mais prolongados de exposição a HG (7h). Além disso, o nosso estudo demonstra que a regulação negativa de Ndr2 influencia a fagocitose, uma das principais funções das células da microglia. Confirmamos também que um ambiente hiperglicémico tem impacto na atividade de células da microglia durante pequenos períodos de incubação. Para as células WT BV-2, foi observado um aumento no ensaio de 4 horas, enquanto no ensaio de 12 horas a atividade fagocitária diminuiu. A fagocitose das células BV-2 com regulação negativa de Ndr2 foi inerentemente menos reativa a alterações nas concentrações de glucose. Este resultado pode ser consequência da desregulação do Ndr2, mas são necessários ensaios adicionais, dada a possível influência de vias de sinalização alternativas na regulação da fagocitose. Também verificámos que a exposição a elevados níveis de glucose e uma regulação negativa de Ndr2 promovem a expressão de TNF- e IL-17a, sugerindo que a cinase NDR2 tem um papel na resposta imune. Por último, a expressão de NDR2 em murganhos diabéticos foi observada na camada plexiforme interna, enquanto em ratinhos não diabéticos, a expressão está presente em todas as camadas da retina, desde a camada nuclear externa até à camada plexiforme interna, sugerindo que as cinases NDR podem ter um papel negativo na regulação da função sináptica e, consequentemente, no processo de informação visual.

Em suma, este estudo revela que NDR2 poderá ter um papel fundamental na retinopatia diabética, afetando as células da microglia e contribuindo para as alterações na retina observadas em doentes diabéticos. É importante ressaltar que são necessários mais ensaios para clarificar as possíveis ligações entre as cinases NDR e as respostas da microglia. Em última análise, a compreensão destes mecanismos moleculares poderá abrir caminho para novos testes genéticos ou estratégias terapêuticas destinadas a atenuar os efeitos da retinopatia diabética e a melhorar a visão dos doentes.

Palavras-Chave: Cinases NDR (Nuclear Dbf2-related), Microglia, Retina, Glucose Elevada, Retinopatia Diabética.

Graphical Abstract:

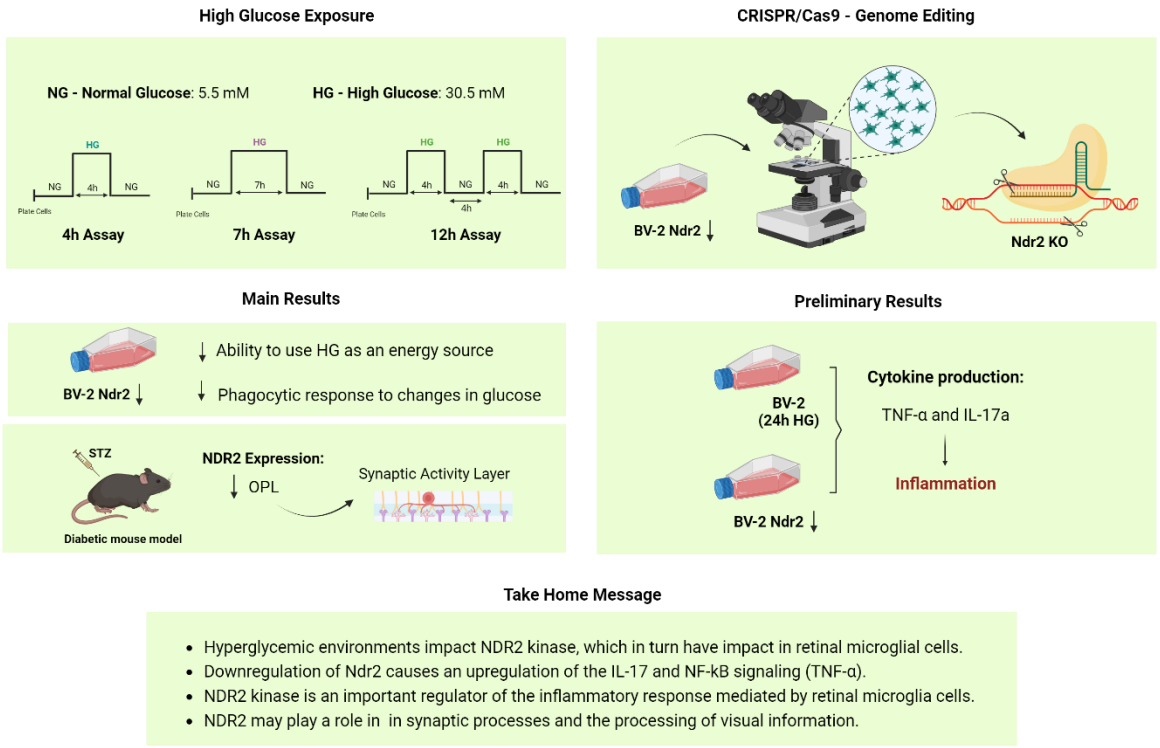

Figure 1 – Graphical Abstract. Graphical abstract representing the main methods, results, and conclusions of this work. (Created with BioRender.com.com).

CHAPTER 1 – Introduction

1.1 Retina

The retina is a part of the central nervous system and plays a crucial role in vision by detecting light and converting it into electrical signals that are send to the brain to create visual perception [1].

The journey of light through the eye begins as it penetrates the cornea, a layer at the front of the eye, and enters the pupil. The amount of light entering the pupil is regulated by the iris. Then, the lens of the eye focuses the light onto the retina. Upon reaching the retina, photoreceptor cells convert the light energy into electrical signals that travel through the interneurons, the ganglion cells, and the optic nerve to the brain. Once in the brain, the signals are translated into images [2] [3].

In the eye, the retina is located at the back part and consists of multiple cell layers and neuronal circuits, which makes it a complex structure. There are 10 layers in the retina. From the innermost layer, we have the internal limiting membrane (ILM), the nerve fiber layer (NFL), the ganglion cell layer (GCL), the inner plexiform layer (IPL), the inner nuclear layer (INL), the outer plexiform layer (OPL), the outer nuclear layer (ONL), the outer limiting membrane (OLM), the photoreceptor layer (PL) and the retinal pigment epithelium (RPE) [4] (Figure 2).

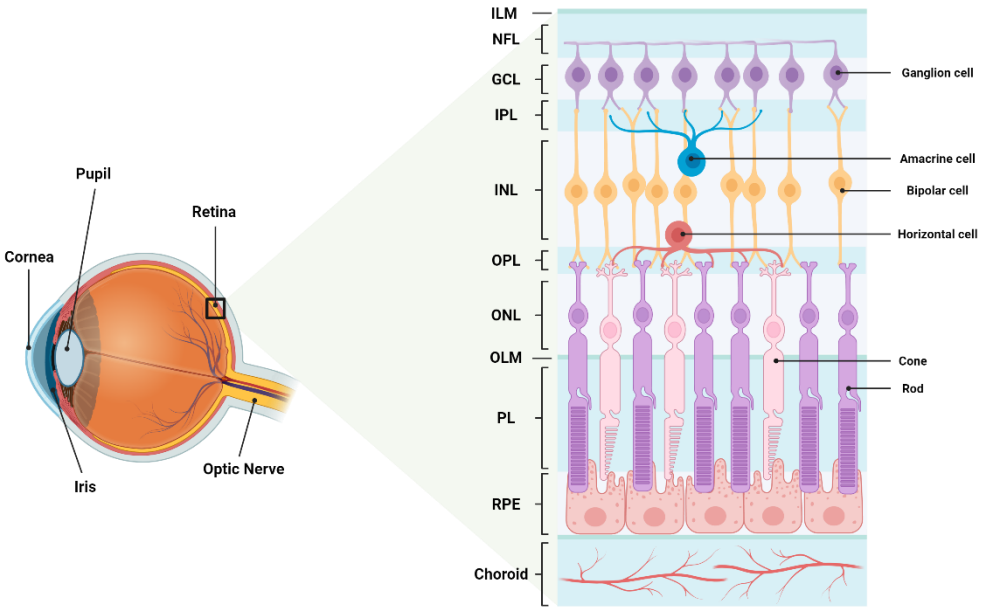

Figure 2- Schematic representation of the retinal structure. Illustration the different layers and cell types. ILM: internal limiting membrane; NFL: nerve fiber layer; GCL: ganglion cell layer; IPL: inner plexiform layer; INL inner nuclear layer; OPL outer plexiform layer; ONL: outer nuclear layer; OLM: outer limiting membrane; PL: photoreceptor layer; RPE: retinal pigment epithelium. (Created with BioRender.com; adapted from [5] with permission)

1.1.1 Retinal Cells

Each of these layers contains different types of cells that work together to maintain the retinal homeostasis, process visual information, and transmit it to the brain. These cells can be grouped into 4 main groups: blood vessels, macroglial cells, neuronal cells, and microglial cells.

1.1.1.1 Vasculature

The blood vessels are tube-like shape structures composed of endothelial cells responsible for the regulation of hemostatic functions, and pericytes that regulate the retinal vascular flow [6]. The retina is a highly vascularized tissue that receives its blood supply from two systems: the central retinal artery and the choroidal vasculature, or choriocapillaris. The central retinal artery enters the eye through the optic nerve and supplies the inner retina, while the choriocapillaris supplies the outer retina, including the photoreceptors. The two systems are interconnected at the level of the RPE. The retinal vasculature is essential for the proper functioning of the retina, as it provides oxygen and nutrients to the retinal cells. In humans, the development of the retinal vasculature is finished before birth [3], [7].

1.1.1.2 Neuronal Cells

The retinal neuronal cells include photoreceptors, bipolar cells, horizontal cells, amacrine cells, and ganglion cells that are responsible for phototransduction, for modulating and for transmitting optical impulses to the brain [6].

Photoreceptors perceive the external light and can be divided into two types: rods and cones. Rods, which constitute the majority of photoreceptors in the human retina, are mainly situated in the outer layers of the retina. They are responsible for low-light vision, resulting in black and white images. Their response time is relatively slow, and they exhibit low contrast sensitivity and spatial acuity. They are not functional during the day, and in the absence of light, they require approximately 40 minutes to become active and enable scotopic vision (black and white). On the other hand, cones are responsible for facilitating color vision, which is also known as photopic vision and is predominantly used during the daytime. These cells can identify three wavelengths of light, including red, green, and blue. They are mainly located in the macula, which is the central area of the retina. The fovea, which is a region within the macula, contains 100% cones and no rods, which allows the brain to distinguish between two points. Unlike rods, cones possess high spatial acuity, can quickly adjust to changes in lighting

conditions, and do not become oversaturated in response to high-contrast light. Both of them release glutamate as their neurotransmitter and synapse into bipolar cells [8]. On the other hand, in mice retina, rods represent 97% of all photoreceptors and cones only identify two wavelengths of light: green and blue.

Among interneurons, bipolar cells, amacrine cells and horizontal cells can be found. Bipolar cells receive inputs from the photoreceptors and are classified into two types: rod bipolar cells, which receive input from rods, and cone bipolar cells, which receive input from cones. By forming a synaptic connection between photoreceptors, these cells facilitate communication between the inner and outer layers of the retina. Bipolar cell bodies are located to the INL while their dendrites and axons form, respectively, the OPL and IPL [8]. As previously mentioned, glutamate is released by both rods and cones, and this release is regulated by light exposure. In the absence of light, there is an increase in glutamate release, leading to excitation of bipolar cells, which are then referred to as off-center bipolar cells. Conversely, in the presence of light, photoreceptors are hyperpolarized and there is a decrease in glutamate release. This type of bipolar cells are known as on-center bipolar cells, as they become active when the light is turned on [9].

Amacrine cells are intermediate neurons whose cell bodies are in the INL and GCL and their dendrites form the IPL. Amacrine cells release inhibitory neurotransmitters like GABA or glycine. They receive excitatory inputs from bipolar cells and send inhibitory outputs to the dendrites of retinal ganglion cells (RGCs), other amacrine cells, and bipolar cells. These outputs have the potential to modulate the activity of RGCs, either by directly inhibiting them postsynaptically or indirectly by inhibiting the bipolar cells terminals presynaptically. [10] Amacrine cells can form functional microcircuits that enable the retina to detect varying shades and movements of light [8].

Horizontal cells are another type of intermediate neurons that have their cell bodies in INL, their dendrites branch in the OPL and communicate with each other through gap-junctions [8]. These cells receive glutamatergic inputs from photoreceptors and send GABAergic inhibitory outputs to both photoreceptors and bipolar cells [11]. Horizontal cells allow the detection, within the same visual field, of objects with different levels of brightness and help the eyes adjusting that and helps to support contrast enhancement [8].

RGCs transmit visual information to the brain by projecting their axons along the optic nerve [12]. RGCs receive chemical signals from amacrines and bipolar cells. These signals are converted into electrical signals through RGCs transmembrane receptors and, depending on

the visual features encoded by RGCs, their axons are directed to specific visual centers in the brain. All the axons of the RGCs are collected into the optic nerve [13].

1.1.1.3 Macroglial and Microglial Cells

Macroglial cells are composed of astrocytes and Müller cells [6]. The astrocytes are almost exclusively confined to the innermost retinal layers [14], namely to the NFL [6]. Since there is a correlation between the distribution of blood vessels and astroglia in the retina, it is believed that astrocytes may enter the retina along with the blood vessels [14]. In terms of function, the astrocytes are important for the development of retinal vascularization, the control of ionic and metabolic homeostasis of RGCs and the regulation of blood flow in the optic nerve [15].

Present in all layers of the retina, from the ILM to the RPE, Müller cells are a type of specialized radial glial cells [15] that constitute approximately 90% of the retinal glia [14]. These cells support the survival of neurons and photoreceptors, providing homeostatic, metabolic, and functional support to them. Additionally, they are also responsible for various other functions including maintaining the structural stability of the retina, preserving and organizing the blood retinal barrier [15], acting as a communication system for metabolic exchange between the vessels and neurons [14], and guiding the light to photoreceptors [15].

The combine action of astroglia and Müller cells in the retina is crucial for several homeostatic functions, such as the elimination of carbon dioxide, maintenance of ion homeostasis, and regulation of extracellular pH [15].

Microglia are another type of glial cells that we can find within the central nervous system, a population of monocytes characterized by their ability to adapt to the surrounding neuronal environment, and due to this feature, they are considered highly plastic cells [14]. Microglia are often referred as the macrophages of the central nervous system, however there are several differences between macrophages and microglial. Macrophages originate from blood monocytes that circulate in the bloodstream and, upon signals of infection or tissue damage, migrate to the affected tissues where differentiate. Furthermore, they are not considered the first line of defense of the central nervous system and do not exhibit responses to calcium levels fluctuations, an hallmark of microglial cells [16]. Microglia are derived from primitive yolk sac progenitors and during the early stages of embryonic development, migrate to the retina [17], [18]. Microglial cells are present in the GCL, IPL, OPL and around the vessels [15].

Adult microglia present a ramified morphology in their inactivated state, and it is widely distributed within the nervous system, being responsible for continuously checking the surrounding environment. When activated, microglia can present antigens, produce pro- and anti-inflammatory cytokines, and reactive oxygen intermediates, as well as gain phagocytic ability [19]. They play a vital role in preserving the functionality of the neuronal network, maintaining tissue homeostasis, clearing cellular debris upon injury, and secreting substances that enable communication between these cells and others [14].

Furthermore, microglia are not only crucial for maintaining retinal homeostasis under normal physiological conditions but also play pivotal roles in various retinal degenerative diseases, including age-related macular degeneration, glaucoma, and diabetic retinopathy (DR) [20].

1.2 Diabetes Mellitus

High blood glucose levels are the defining feature of diabetes mellitus, a group of chronic metabolic diseases that can lead to a variety of other pathologies, including diabetic retinopathy [21] .

Type 1 and type 2 diabetes are the two main types of diabetes. Type 1 diabetes occurs when the body doesn't produce insulin or produces very low amounts, which results in the need of insulin injections to regulate blood glucose levels [22]. This is caused by an autoimmune reaction that destroys pancreatic beta cells [21], and children and young adults are the most affected. Type 2 diabetes is the most prevalent form of diabetes and occurs when the body loses the ability to respond to insulin as a result of insulin resistance. Although it is more often diagnosed in older adults, there is an increasing number of type 2 diabetes cases in young people related to obesity. The treatment for this patients includes following a healthy lifestyle and may also require oral medication and insulin [22].

1.2.1 Diabetic Retinopathy

Diabetes is a major risk factor for the occurrence and progression of neurovascular damage in the retina [23]. Studies suggest that, in Europe, approximately 20%-35% of diabetic people will develop any form of diabetic retinopathy, which is the most common microvascular complication of diabetes [24].

1.2.1.1 Pathological Insights of Diabetic Retinopathy

Diabetic retinopathy is a neurodegenerative disease characterized by microvascular lesions in the retina that can lead to visual loss [25], [26]. Optical examination can identify the early stage of DR, known as non-proliferative diabetic retinopathy (NPRP) [27]. This one includes enhanced vascular permeability and capillarity occlusions, [28] microaneurysms, and microhemorrhages [27]. When DR is in an advanced stage, it is called proliferative diabetic retinopathy (PDR), which is characterized by neovascularization and the formation of new blood vessels which result in detachment of the retina and vision impairment [27], [28]. Another significant stage of DR, and the main cause of blindness [27], is diabetic macular edema (DME), a complication where the breakdown of the BRB leads to thickening of the macula due to the accumulation of extracellular fluid [26].

The maintenance of BRB is achieved by the blood vessels of the retina, which present tight junctions that prevent them from leaking. When exposed to high glucose levels, these tight junctions are damaged, causing the leaking of blood into the retina [29]. Normally, the ratio of endothelial cells to pericytes, the two types of cells that constitute the blood vessel, is 1:1; however, in DR, there is a loss of pericytes, and the ratio changes to 4:1. Since pericytes are responsible for capillary support, this event leads to their death and consequently to ischemia and microaneurysms [28], [29]. When this occurs, pro-angiogenic cytokines are released, resulting in pathologic neovascularization, in which new vessels grow on the surface of the retina towards the vitreous, causing retinal detachment [29], [30]. When cytokines and other molecules are released, leukocytes are recruited and, under hyperglycemia conditions, they adhere to the vascular endothelium causing leukostasis. Inflammatory cytokines and vascular permeability factors are also released by white blood cells, which result in endothelial junctions disruption and BRB destruction [25].

1.2.1.2 Hyperglycemia in DR: Inflammation and Oxidative Stress

The impact of hyperglycemia on the development and progression of diabetic retinopathy has been extensively studied, highlighting its central role in the pathophysiology of this ocular complication. Chronic hyperglycemia is probably the main cause of DR [31], and it is linked to low-grade inflammation that is reflected by the release of higher amounts of pro-inflammatory mediators [23]. Indeed, many studies have shown increased levels of tumor necrosis factor-alpha (TNF-α) and interleukins (IL)-1β , IL-6, and IL-8 in the retina and vitreous of patients with DR [32]–[34] and animal models of diabetes [35], [36].

A hyperglycemic environment can also induce cellular oxidative stress, an imbalance between the production and elimination of oxygen reactive species (ROS) [29], followed by nuclear factor kappa B (NF-κB) activation, pro-inflammatory cytokines release, microglia activation, and culminating in inflammatory exacerbation and cell death [31]. It has been shown that NF-kB activity is increased in different types of retinal cells of animal models of diabetes and diabetic people [37], [38].

1.2.2 Microglia and Inflammation

Microglia can be found in two distinct phenotypes, characterized as pro-inflammatory and anti-inflammatory states. To maintain homeostasis, microglia transit to the anti-inflammatory state, releasing anti-inflammatory cytokines. However, upon detection of danger signals, microglia undergo a shift towards a pro-inflammatory state, releasing pro-inflammatory cytokines. Once the danger is solved, microglia return to a surveillance state [39]. Usually, the inflammation induced by activated microglia presents protective properties, but under continuous and prolonged stress, microglia become overly reactive and release excessive pro-inflammatory molecules and neurotoxic substances, leading to several complications and damage to the central nervous system [31]. The microglial states are intricately regulated by numerous signaling pathways, contributing to their diverse functions in response to various stimuli.

1.3 NDR Kinases

Nuclear Dbf2-related (NDR) kinases are a family of serine-threonine protein kinases and key effectors of the Hippo pathway, a highly conserved signaling pathway, first discover as a regulator of cell proliferation, differentiation, and apoptosis. These kinases have been identified in a wide range of taxa, spanning from unicellular organisms like yeast to multicellular organisms like plants, animals and humans [40]. In this family, there are four NDR kinases: NDR1 and NDR2 (NDR1/2), also known as serine-threonine kinase 38 (STK38) and serine-threonine kinase 38 like (STK38L), respectively and large tumor suppressor (LATS) 1 and LATS2 [41]. LATS1 and LATS2 are more studied and considered the canonical branch of the Hippo pathway, while NDR1 and NDR2 are understudied and considered the noncanonical branch of the Hippo pathway.

1.3.1 NDR Kinases and the Hippo Pathway

The Hippo pathway is activated by a cascade of signaling events that culminate in the phosphorylation and regulation of several substrates, like Yes-associated protein (YAP) and WW Domain Containing Transcription Regulator1 (TAZ), the main substrates of this pathway. When phosphorylated, YAP/TAZ are targeted for degradation or retained in the cytoplasm, and when dephosphorylated, these co-transcription factors translocate to the nucleus and modulate the expression of target genes. The NDR kinases have been shown to phosphorylate YAP and TAZ, leading to their cytoplasmic sequestration and degradation, thereby inhibiting their activity (Figure 3). However, in the recent years, more substrates of the NDR kinases have been discovered including NF-kB, BECLIN1, RAPH1 and many more [41].

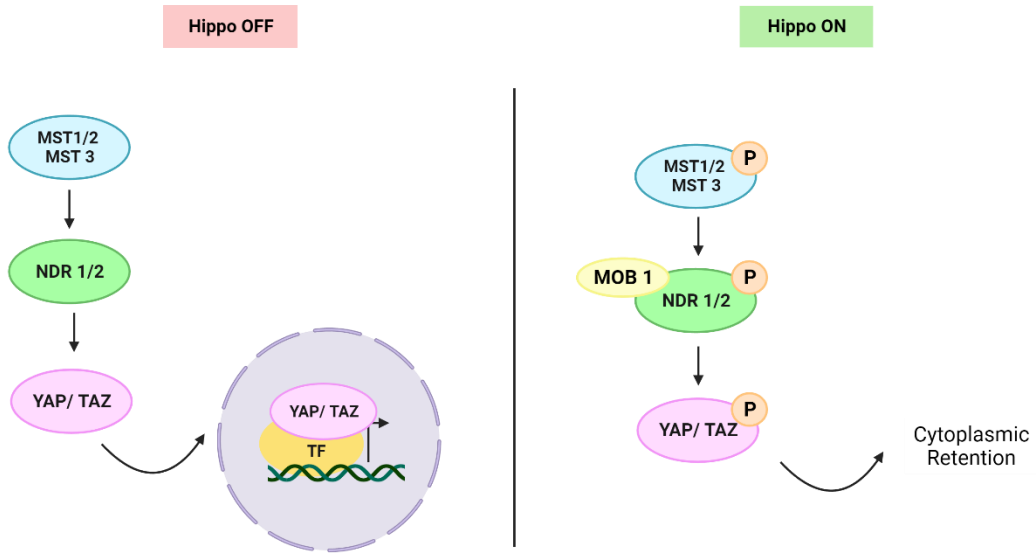

Figure 3 – Role of NDR kinases in the regulation of the Hippo Pathway. When the Hippo Pathway is OFF, NDR kinases are dephosphorylated, and YAP/TAZ translocate to the nucleus and modulate the expression of target genes. When the Hippo Pathway is ON, NDR kinases are phosphorylated, and consequently, YAP/TAZ will be phosphorylated, leading to their cytoplasmic retention. (Created with BioRender.com)

1.3.2 NDR kinases: Structure and Regulatory Mechanisms

Mammalian NDR1 and NDR2 kinases exhibit a high degree of protein sequence similarity, sharing approximately 90% of their sequence, to the exception of a peptide located between amino acids 2 and 23 and between amino acids 420 and 434. Both kinases consist of 14 exons with conserved intron-exon boundaries [41] and present typical features of the AGC

kinases group, including an activation segment and hydrophobic-motif regulatory-phosphorylation sites. However, what distinguishes them to the other AGC group kinases is the presence of a conserved N-terminal regulatory (NTR) domain and an insert of 30–60 residues between subdomains VII and VIII, which doesn't seem to be conserved. NDR2 is mostly reported to be a cytoplasmic and membranous protein, whereas NDR1 is mostly defined as a nuclear kinase. However, recent studies also define NDR1 as a cytoplasmic protein [42].

The activation mechanisms of NDR kinases involve multiple regulatory processes, including phosphorylation events and protein-protein interactions. These kinases are primarily activated through phosphorylation at specific sites within the activation segment and the hydrophobic-motif by upstream kinases, like Mammalian STE20-like (MST) kinase and LATS. Additionally, their activation can be influenced by binding molecules such as Mps1-one binder (MOB1), a co-activator that facilitates phosphorylation by other kinases. In addition, NDR kinases can undergo conformational changes in response to various stimuli, further modulating their activity [40], [42].

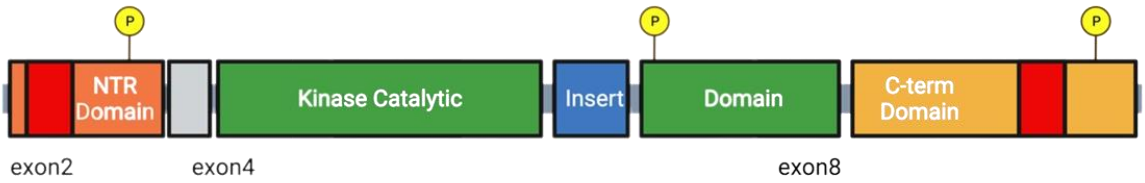

Figure 4 – Schematic representation of NDR protein structure. The two regions that differ between NDR1 and NDR2 are represented in red, and the regulatory-phosphorylation sites are represented by the yellow circles. (Created with BioRender.com)

1.3.3 NDR Kinases and Inflammation

Recent research has highlighted the involvement of Hippo signaling components in both innate and adaptive immunity. Among these components, NDR1/2 has emerged as a significant player in inflammation and displays a distinct role in modulating inflammatory responses. NDR1 promotes TNFα-induced NF-κB activation through its kinase activity and interaction with multiple signal components within the NF-κB pathway, thus acting as a positive regulator in TNFα-induced inflammation. Conversely, NDR2 acts as an inhibitor of

IL-17 signaling. However, in retinal inflammation, the role of NDR kinases remains unknown [41], [43].

1.4 CRISPR/Cas9 – Genome Editing

Genome editing is a biotechnology technique that can be applied to the genetic engineering of living cells by inserting, deleting, or replacing DNA in a specific position within the genome [44].

One of the most modern and recent tools for genome engineering is CRISPR/Cas, a virus-resistant adaptive immune system of prokaryotes. CRISPR (Clustered Regularly Interspaced Short Palindromic Repeat) is an organization of short and repeated DNA sequences interspaced within the bacteria or archaea genome [45], [46]. This system allows the insertion of fragments of viral DNA in a region denominated CRISPR array and function as a genetic memory that protects the cells from repeated attacks. Virus fragment cleavage is accomplished by the Cas (CRISPR-associated) enzyme [46].

1.4.1 Molecular Components and Mechanisms

There are two different classes of this system. The class I employs large multi-Cas protein complexes, while the class II only uses a single endonuclease. There are various types within each class, and type II, which uses Cas9, is one of the best characterized [46], [47].

The guide RNA (gRNA) and the Cas9 enzyme are the two basic components of CRISPR/Cas9. Two different parts that form the gRNA are: the CRISPR RNA (crRNA), which has a complementary sequence to the target DNA and can pair with it, and the trans-activating CRISPR RNA (tracrRNA), which acts as a binding scaffold for Cas9 endonuclease [46]. For genome editing, these two parts can be fused together in order to generate a chimeric single-guide RNA (sgRNA) that can target any gene sequence [48]. Cas9 is a large, multi-domain DNA endonuclease that was extracted from *Streptococcus pyogenes*. As an endonuclease, this enzyme acts like a scissor and is responsible for cutting the two strands of target DNA that is complementary to the gRNA sequence. In the absence of the gRNA, Cas9 remains inactive. It is divided into two different regions, the recognition (REC) lobe and the nuclease (NUC) lobe [46]. The first one can be subdivided into two other domains (REC I and REC II) that are responsible for binding to the gRNA and the NUC lobe is composed of RuvC, HNH, and Protospacer Adjacent Motif (PAM) interacting (PI) domains. The complementary sequence of the crRNA is cleaved by the HNH domain, while the opposite

strand is cleaved by the RuvC domain [49]. The functionality of CRISPR/Cas9 requires a short and conserved DNA sequence downstream to the target site, known as PAM [46]. The sgRNA only connects with the target DNA after the identification of a correct PAM sequence, otherwise there will be a dissociation between the enzyme and the DNA [47]. The function of PAM is to distinguish between foreign genetic material, non-self-sequence, and the DNA sequence present in CRISPR arrays, self-sequence. This is a crucial mechanism that prevents the CISPR/Cas system from targeting their own CRISPR arrays, which could trigger an autoimmune response [50]. All Cas endonucleases have a distinct PAM sequence that varies in length and complexity. In the case of the widely used Cas9 enzyme, that sequence is 5`-NGG-3` (N can be any DNA base) [47], [50].

The sgRNA recognizes the target sequence via the complementary crRNA and directs Cas9 to the site of interest. Cas9 is activated when the PAM sequence is recognized, and HNH and RuvC cleave both strands of DNA, generating a blunt-ended double-strand break (DSB) that will be repaired by the host`s cellular machinery [46], [47].

There are two main mechanisms to repair DNA: non-homologous end joining (NHEJ) and homology-directed repair (HDR). The NHEJ can occur at any phase of the cell cycle, and the DNA is repaired through an error-prone mechanism that can lead to random insertions, deletions, or substitutions that generate a mutation in the DNA. In contrast, the HDR uses a homologous DNA template containing the desired sequence of interest, leading to a precise gene insertion or replacement. This one is active during the late S and G2 phases of the cell cycle [46], [49] (Figure 5).

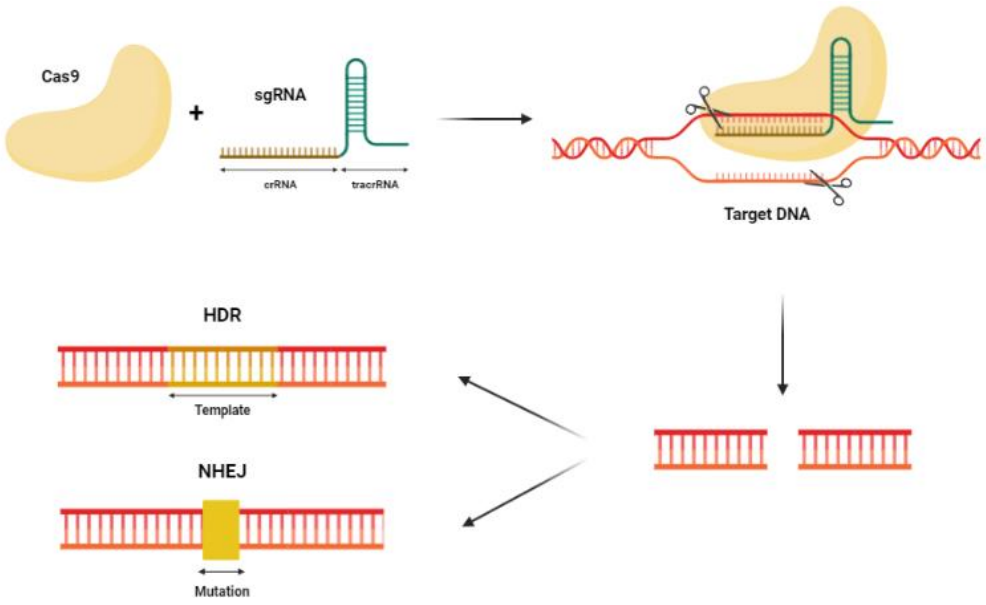

Figure 5 – Schematic representation of how the CRISPR/Cas9 system works. The CRISPR-Cas9 system consists of two key molecules that introduce a change in DNA: an enzyme called Cas9, which acts like a pair of 'molecular scissors' and can cut the two strands of DNA at a specific location, and a guide RNA, a complementary sequence of the target DNA that ensures that the Cas9 enzyme cuts at the right point in the genome. (Created with BioRender.com; adapted from [51] with permission)

1.5 Aims of the study

Diabetes is a major risk factor for the occurrence and progression of neurovascular damage in the retina, leading to diabetic retinopathy. Microglial cells are a key player in the retinal response and become activated in response to various pathological stimuli, including hyperglycemia. Furthermore, the influence of hyperglycemia on microglial cells is particularly well explore under prolonged and chronic conditions. NDR kinases are known to have a role in neuroinflammation and neurodegenerative diseases, pointing to their potential involvement in the pathophysiology of diabetic retinopathy. However, the precise role of NDR kinases in the context of retinal microglial responses to hyperglycemia remains largely unexplored.

With these considerations in mind, our study pretends to uncover the impact of short-term high glucose exposures on NDR kinases within microglial cells. To accomplish that, we evaluated protein expression by western blot and immunocytochemistry and mRNA expression levels by qRT-PCR. Additionally, our study extends to comprehending the consequences of high glucose fluctuations on microglial cells in the absence of Ndr2. To achieve that goal, we first set up a CRISPR-Cas9 strategy to delete Ndr2 gene in BV-2 cells validated by qRT-PCR and immunohistochemistry. Subsequently, we compared the phagocytosis, migration, and pro-inflammatory cytokines expression of these genetically

modified microglial cells with those of wild-type (WT) BV-2 cells. Finally, we set up the first steps of studying the effect of the deletion of Ndr2 gene in the retina of diabetic mice.

In essence, this work intends to fill the gap in understanding the intricate interactions between hyperglycemia, retinal microglia, and NDR kinases, hopping to contribute to a deeper comprehension of the underlying mechanisms and potentially unveil novel therapeutic approaches for handling the pathophysiological consequences of diabetic retinopathy.

CHAPTER 2 – Methods and Materials

2.1 *In vitro* studies

The in vitro part of this project was performed with immortalized murine microglial cell line BV-2. BV-2 cells are generated from C57/BL6 mice brain microglial immortalized by a v-raf/v-myc carrying J2 retrovirus and are commonly used as a replacement for primary microglia [52]. For the experiments, we chose to use BV-2 cell line instead of primary microglia due to its ready availability, consistent characteristics, cost-effectiveness and to reduce animal sacrifice. By doing so, we are implementing the initial "R" of the 3Rs principle: Replacement, Reduction, and Refinement, wherein "replacement" stands for finding alternatives to minimize animal involvement in experiments whenever possible [53].

2.1.1 BV-2 Cell Culture

BV-2 cells were cultured in Roswell Park Memorial Institute culture medium (RPMI; Gibco, UK) supplemented with 10% (v/v) Fetal Bovine Serum (FBS; Gibco, Germany), 1% (v/v) L-glutamine (Gibco, USA), and 1% (v/v) Penicillin-Streptomycin (Pen/Strep; Gibco, USA). The medium was always pre-heated at 37 °C.

The cells were grown in a 75 cm^2 flask, and cell passage and splitting were performed when cells reached confluency, which was assessed through a light optical microscope.

For cell passage and splitting, the growth medium in the flask was discarded and 8 mL of new growth medium was added. The cells were detached by vigorous tapping of the flask.

Cellular viability and density were determined by a viable cell count using Trypan Blue (Sigma, UK) staining. The cells were diluted 1:1 in Trypan Blue and placed in a hemocytometer under an optical microscope for counting. After cell counting, the cells were either split in a ratio of 1:10 into a 75 cm^2 flask or seeded into multi-well cell culture plates to be used for subsequent experiments.

Cells were then maintained in RPMI at 37 °C in a humidified atmosphere with 5% CO_2 and kept until passage 26 (P26).

2.1.2 High Glucose Exposure

BV-2 cells were seeded at a density of 1.0×10^4 cells / cm^2 with 3 mL of medium or 1 mL of medium into 6 or 12 multi-well cell culture plates, respectively, in Dulbecco's Modified Eagle

Medium (DMEM; Gibco, UK), supplemented with 10% (v/v) FBS, 1% (v/v) L-glutamine, and 1% (v/v) Pen/Strep.

After 16h-18h, the culture medium was supplemented with 25 mM D-glucose (Sigma, USA) in addition to the 5.5 mM already present in DMEM, reaching a final concentration of 30.5 mM (HG) to simulate hyperglycemic conditions observed in diabetes.

The cells were exposed to HG for 4h, 7h or 2 times 4h with intervals of 4h between exposures. Then, BV-2 were kept in normal glucose (5.5 mM glucose, NG) medium until the next morning for subsequent experiments (Figure 6).

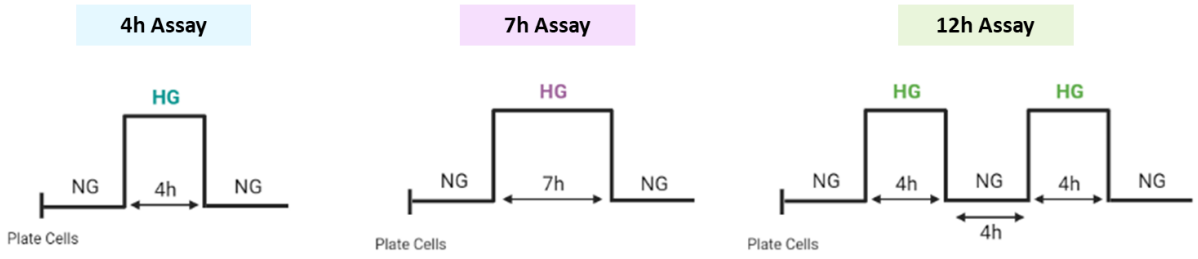

Figure 6 – Schematic representation of the different timepoints used for the experiments. BV-2 cell cultures were incubated in 5 mM glucose (NG) or 30 mM glucose (HG) for different timepoints: 4h (4h Assay) , 7h (7h Assay) or two times 4h HG with a break of 4h in between (12h Assay). (Created with BioRender.com)

2.1.3 SDS-PAGE and Western Blot

After the HG incubations, cells cultured in 6 multi-well plates were removed from the incubator and rapidly placed on ice. The culture medium was removed, and the cells were washed three times with ice-cold Phosphate-buffered saline (PBS; 137 mM NaCl, 2.7 mM KCl, 1.8 mM KH_2PO_4, 10 mM Na_2HPO_4; pH 7.4). Then BV-2 cells were lysed with 100 µL of ripa lysis buffer (150 mM NaCl, 50 mM Tris, 5 mM EGTA, 0.5% sodium deoxycholate, 0.1% SDS, 1% triton X-100, 1 M DTT: Milli-Q H_2O; pH 7.5), supplemented with 10% protease inhibitor (cOmplete™, EDTA-free Protease Inhibitor Cocktail; Roche, Germany), and detached with a cell scrapper.

The obtained suspension was sonicated on ice three times with 5 sec pulses and kept on ice for 30 min. To separate the protein lysate from the cell debris, a centrifugation was performed (16 000 x g / 10 min / 4 °C). The protein concentration was determined by the bicinchoninic acid (BCA) method using the BCA protein kit and its recommended protocol. (Pierce Biotechnology, USA) The protein extracts were denatured at 95°C for 10 min in 1:5

(v/v) sample buffer 6X (0.5 M Tris, 30% glycerol, 10% SDS, 0.6 M DTT, and 0.012% bromophenol blue; pH 6.8), and stored at - 80 °C.

Stacking (4%) and resolving (12%) sodium dodecyl sulphate (SDS) polyacrylamide gels were prepared to separate the protein by electrophoresis. On the day of the experiment, 20 µg of protein were separated on an SDS-polyacrylamide gel and submerged in electrophoresis buffer (25 mM Tris, 192 mM glycine, 0.1% SDS) at 85 V for 20 min and then at 150 V for 1 h. While the electrophoresis was running, the PVDF membranes (polyvinylidene difluoride), (Millipore, Spain) were activated in 100% methanol for 2 min, followed by 2 min in H_2O and more than 5 min in CAPS buffer (3-[Cyclohexylamino]-1-propanesulfonic acid, 10 mM) supplemented with 10% methanol (transfer buffer). The separated proteins were transferred onto a PVDF membrane, sandwiched between two sponges and two transfer papers, and submerged in transfer buffer at 0.75 A for 2 h.

After that, membranes were blocked in 5% (w/v) low-fat dry milk (Nestlé, Switzerland) / Tris-buffered saline (TBS; 200 mM Tris HCl, 1.37 mM NaCl) with 0.1% (v/v) Tween 20 (TBS-T) for 1 h, under continuous agitation. Primary antibodies (Table 1) were diluted in TBS-T containing 5% (w/v) low-fat dry milk, and the membranes were incubated overnight at 4 °C under continuous agitation. On the next day, membranes were washed with TBS-T, 3 times for 10 min each time, and then incubated with the secondary antibody (Table 2), diluted in 5% milk / TBS-T (w/v), for 1 h at room temperature (RT), under continuous agitation. Once again, the membranes were washed with TBS-T, 3 times for 10 min each time, and then chemiluminescence was detected by ImageQuantTM LAS 500 (GE Healthcare, USA) using the western-bright ECL KIT (Advansta, USA). Band intensity was quantified through ImageJ (National Institutes of Health, US).

2.1.4 RNA Extraction

After the HG experiments, cells cultured in 6 multi-well plates were removed from the incubator, and the RNA was extracted using a column-based RNA purification kit (RNeasy Mini Kit, Qiagen), following the manufacturer`s provided protocol for adherent cells.

Isolated RNA was then eluted in 30 µL of RNase-free water, and RNA concentration and sample purity were assessed by UV-visible spectroscopy in an automated NanoDro One Microvolume UV-Vis Spectrophotometer (Thermo Fisher Scientific, USA).

The NanoDrop was also used to determine the ratio of absorbance at 260 and 280 nm (A260/280) and the ratio of absorbance at 260 and 230 nm (A260/230) to assess the purity of the isolated nucleic acid and contamination with proteins, phenolates, and thiocyanates resulting from the isolation protocol. For cDNA synthesis, samples were considered suitable when the ratio values for both A260/A280 and A260/A230 were within the range of 1.8 to 2.2.

2.1.5 Complementary DNA (cDNA) synthesis and Quantitative reverse transcription PCR (qRT-PCR)

After RNA extraction, cDNA was synthesized using the NZY First-Strand cDNA Synthesis Kit (Nzytech, Lisbon), following the manufacturer's instructions. The resulting cDNA was diluted to a final concentration of 25 ng/µL, and then used for the amplification of the desired genes using the iTaq™ Universal SYBR® Green Supermix (Bio-Rad Laboratories, USA), which contains all the necessary components for qRT-PCR. The reactions were carried out in duplicate, following a 3-steps protocol: 15 sec denaturation step at 95 °C, followed by 30 sec at 60 °C for the annealing step, and lastly a 30 sec step at 72°C for elongation, using the QuantStudio 3 Real-Time PCR System (Thermo Fisher Scientific, USA).

The PCR reaction mix contained 2 µl of cDNA, 2 µL of 10 mM of each specific primer set (Table 3), 6 µl of RNase-free water, and 10 µl of iTaq™ Universal SYBR® Green Supermix, for a final volume of 20 µl.

2.1.6 Resazurin Viability Assay

Resazurin is a redox indicator that can permeate cells and be introduced directly into cell cultures. Viable cells with an active metabolism are able to reduce the blue resazurin to the pink resorufin product. The amount of resorufin, which can be detected by the change in absorbance at 570 nm and 620 nm, is directly proportional to the number of viable cells [54] (Figure 7).

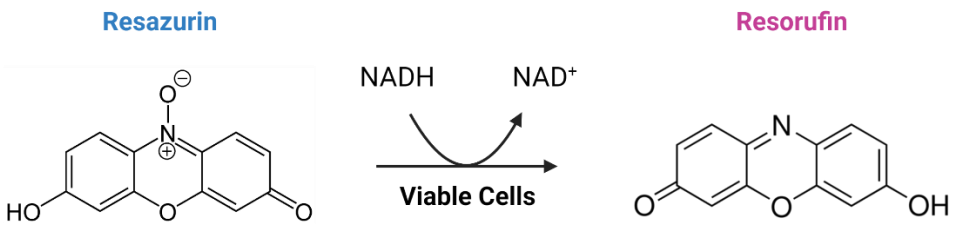

Figure 7 – Schematic representation of resazurin viability test. (Created with BioRender.com)

To access the viability of BV-2 cells, after HG assays, resazurin, diluted in PBS (Sigma, USA) at 500 µM was added to the cells to a final concentration of 50 µM. Following a 4h incubation at 37 °C and 5% CO_2, the absorbance at 570 nm and 620 nm was measured by a multimode microplate reader (Agilent Technologies, USA). The normal medium served as the blank condition to eliminate background absorbance. By analyzing the absorbance values, the percentage of cell viability can be determined.

2.1.7 Immunocytochemistry

Following the resazurin assay, the cells were washed 3 times with PBS before being fixed with 100% methanol at -20 °C for 10 minutes at RT. Subsequently, the cells were washed again 3 times with PBS and then permeabilized and blocked with a solution containing 3% Bovine Serum Albumin (BSA) and 0.25% Triton X-100 in PBS for 30 minutes.

After that, we incubated the cells with the primary antibody (Table 1) in a blocking solution, overnight at 4 °C. The next day, cells were washed 3 times with PBS and incubated with the secondary antibody (Table 2) and DAPI (0.5 µg/mL; Invitrogen at 5 mg/mL, USA) for 1h. Finally, the cells were washed again 3 times with PBS, once with Milli-Q Water (mqH_2O), and mounted on slides using a fluorescence mounting medium (Dako, Denmark). Fluorescence was assessed using a fluorescence microscope (Axio Observer.Z1, Germany) and analyzed with ImageJ (National Institutes of Health, US).

2.1.8 Immunohistochemistry

Cryosections were fixed with acetone at -20°C for 10 min followed by a rehydration in PBS twice for 5 min. Subsequently, they were delineated with a PanPen, permeabilized for 30 min with 0.25 triton X-100 / PBS, blocked in 10% normal goat serum (Sigma, USA) and 1% BSA /

PBS for another 30 min, and incubated, overnight at 4°C, with the primary antibody (Table 1). The next day, cryosections were washed 3 times for 10 min with PBS and incubated for 60 min at RT with the secondary antibody (Table 2) and DAPI (0.5 µg/mL). Then they were washed again 3 times for 10 min with PBS, mounted with fluorescence mounting medium and covered with a coverslip. Fluorescence was assessed using a fluorescence microscope and analyzed with ImageJ.

Table 1 – List of primary antibodies used for different experiments. Western blot (WB), Immunocytochemistry (ICC) and Immunohistochemistry (IHH).

Primary Antibodies						
Name	**Type**	**Host**	**Dilution**	**Assay**	**Company**	**Reference**
Anti-Ndr 1/2	Monoclonal	Mouse	1:1000	WB	Santa Cruz	sc-271703
Anti-Calnexin	Polyclonal	Goat	1:10 000	WB	Sicgen	AB0041-500
Anti-Ndr 1/2	Monoclonal	Mouse	1:100	ICC	Santa Cruz	sc-271703
Anti-Iba1	Polyclonal	Rabbit	1:500	IHC	Wako	019-19741
Anti-Ndr 2	Polyclonal	Rabbit	1:100	ICC and IHC	Wako	019-19741

Table 2 – List of secondary antibodies used for different experiments. Western blot (WB), Immunocytochemistry (ICC) and Immunohistochemistry (IHH).

Secondary Antibodies						
Name	**Type**	**Host**	**Dilution**	**Assay**	**Company**	**Reference**
HRP Anti-Mouse	Polyclonal	Goat	1:10000	WB	Bio-rad	1706516
HRP Anti-Goat	Polyclonal	Rabbit	1:10000	WB	Alfagene	LTI 611620
Alexa Fluor 488 Anti-Mouse IgG (H+L)	Polyclonal	Goat	1:1000	ICC	Invitrogen	A11001
Alexa Fluor 568 Anti-Rabbit IgG (H+L)	Polyclonal	Goat	1:1000	ICC and IHC	Invitrogen	A11036
Alexa Fluor 488 Anti-Rabbit IgG (H+L)	Polyclonal	Goat	1:1000	ICC and IHC	Invitrogen	A11008

2.1.9 Phagocytic Activity Assay

Under aseptic conditions, fluorescent yellow-green latex beads (0.0025%; Sigma, USA) were added to the cells following HG experiments and incubated for 1h at 37 °C with 5% CO_2. Then the cells were fixed with 100% methanol at -20 °C for 10 min and after being washed 3 times with PBS, the cells were permeabilized and block with a solution of PBS with 3% BSA and 1% triton X-100, for 30 min. The coverslips were then washed again and incubated for 30 min with DAPI (1:10000) and phalloidin (1:500; Sigma, USA). Finally, and after an additional wash with PBS and mqH_2O, coverslips were mounted on slides using fluorescence mounting medium. The fluorescence was assessed using a fluorescent microscope, and the analysis was performed through ImageJ.

2.1.10 Migration Assay

After 4h of HG exposure, cells cultured in 6 multi-well plates were removed from the incubator. Under aseptic conditions, the medium was removed, and cells were washed with PBS. Subsequently, a scratch was made on the bottom of each well using a vertically held tip to clear cells from the scratched area, followed by another PBS wash. Two microscope snapshots were captured, one immediately after the scratch and another four hours later. Before cell plating, reference lines were drawn on the bottom of each well to ensure that the pictures were taken at the same position (Figure 8). The number of cells in the wound area was counted before and after migration in a limited area of approximately 900x900 pixels, set up within the scratch wound. The number of cells within that area after migration was counted using the plugin "Analyze Particles" of ImageJ.

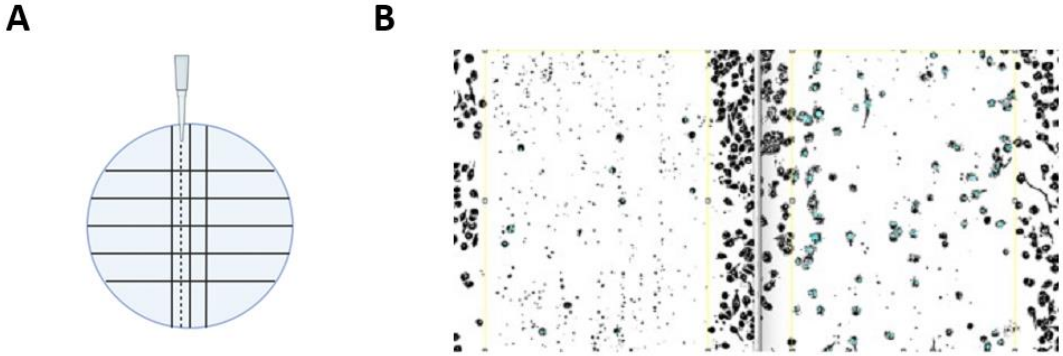

Figure 8 – Schematic representation of the lines drawn at the bottom of each well for the migration assay and images obtained after software analysis. (A) The lines were drawn to help with spatial localization under the microscope and allowed us to take pictures at the same location. The scratch wound (broken line) was made between two

vertical lines, and pictures were taken at an intersection between one horizontal line and one vertical line. **(B)** Images originated after ImageJ analysis. The blue dots represent the cells that the software has identified and counted. In the left side is the picture taken immediately before scratch wound and the one on the right side is the picture taken after 4h incubation. Only cells within the yellow rectangle can be counted by the software. (Created with BioRender.com)

CLONING

2.1.11 Ligation and digestion

The sgRNA was designed using the ChopChop program to target the exon 8, and ordered through NZYTech; (sgRNA #8, GCAAACTTACAGAAGTCGCTTGG, in green PAM sequence).

To initiate primer annealing, the forward and reverse primers were combined in equal concentrations with T4 buffer, DEPC H2O, and T4 PNK (NEB, USA). The mixture was then subjected to incubation at 37°C for 30 minutes, followed by a subsequent incubation at 95°C for 5 minutes. The temperature gradually decreased at a rate of 5°C per minute until it reached 25°C. This step serves to obtain ds-gRNA. The resulting product was purified through the PureLink™ Quick Gel Extraction and PCR Purification Combo Kit (Invitrogen, LT), following the protocol provided by the manufacturer. Subsequently, the px459 plasmid (hSpCas9-2A-Puro V2.0, Addgene, UK) was digested using the BbS1 restriction enzyme (NEB, USA) and combined with the purified ds-gRNA in a ligation reaction mixture containing a T7 DNA ligase (NEB, USA) and the appropriate ligation buffer. The ligation reaction was then incubated overnight at 16°C (Figure 9).

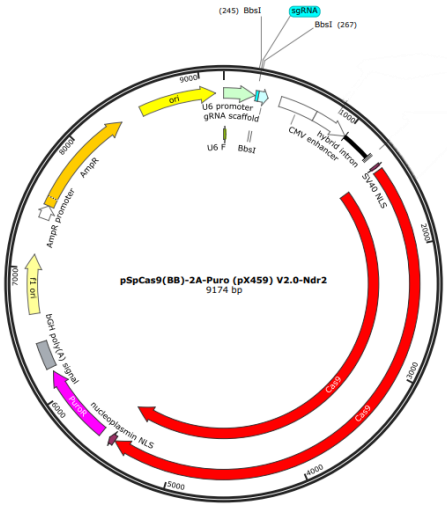

Figure 9 – Schematic representation of the plasmid used for CRISPR-Cas9 strategy. AmpR – ampicillin resistance gene; PuroR – puromycin resistance gene; Cas9 – CRISPR associated protein 9.

Unfortunately, that sgRNA was proven to target several other genes with a query cover superior at 65%. The transfected cells presented an abnormal phenotype characterized by a high incidence of apoptosis, which contradicted the anticipated outcome of Ndr2 tumor suppressor deletion. Another sgRNA construction (sgRNA #7, CCA GACAACCTTTTACTGGATGC, in green PAM sequence) designed using the ChopChop program and subsequently cloned into the pRP[CRISPR]-Puro-hCas9-U6 vector by VectorBuilder was used. The sgRNA #7 was designed to target exon 7, which codes for the kinase domain of NDR2 protein (Figure 10).

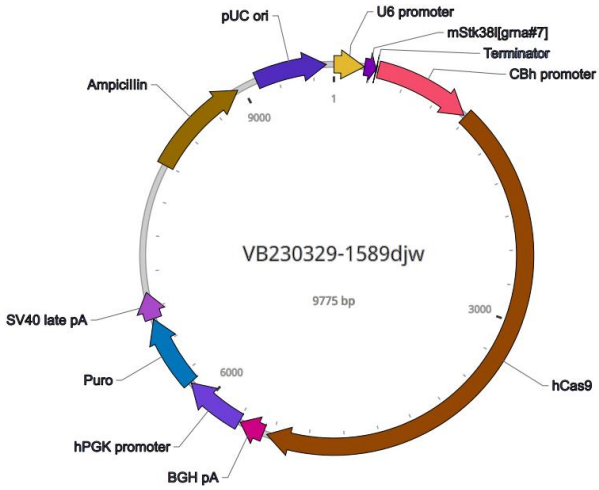

Figure 10 – Vector map of the sgRNA #7 used to perform CRISPR-Cas9 strategy. Ampicillin – ampicillin resistance gene; Puro – puromycin resistance gene; hCas9 – CRISPR associated protein 9.

2.1.12 Transformation

The plasmid of interest was added to DH5α competent bacteria (Invitrogen, USA & Canada) and kept on ice for 30 min. After that, the mix was transferred to a 42°C water bath for 1 min and then to ice for 5 min to create a thermal shock and facilitate the integration of the plasmid into the bacteria. To recover the bacteria, 200 µL of S.O.C. medium (Invitrogen, UK) was added and incubated at 37°C for 25 minutes. Finally, the entire volume was plated onto LB Agar plates with ampicillin and incubated at 37°C overnight.

2.1.13 Mini-Culture

After transformation, several colonies were selected and grown in LB Broth medium (VWR, USA) with ampicillin at 37 °C under agitation conditions, overnight.

2.1.14 Miniprep

After mini-culture and in order to extract the plasmids from bacteria, the QIAprep Spin Miniprep Kit (Qiagen, Germany) was used, and the manufacturer's instructions were followed.

2.1.15 Sequencing DNA preparation

After extracting and purifying DNA from multiple mini cultures, the plasmids were prepared for sequencing. For that 50-100 ng/μL of plasmid DNA were mixed along with 5 μL of primer U6F (Table 3) at 5 pmol/μl. Subsequently, the samples were sent to Eurofins for Sanger sequencing analysis.

CRISPR/CAS9 GENE EDITING

2.1.16 Transfection

Lipofection or liposome transfection is a technique that uses positively charged cationic lipids to introduce genetic material into cells. Lipofectamine, a commonly used cationic lipid, exhibits broad applicability in vitro across a wide range of cell types [55]. By forming complexes with negatively charged nucleic acids, lipofectamine aids their fusion across cell membranes [46], [56].

BV-2 cells were seeded into a T25 flask, at a density of 2 x 10^4 cells / cm^2 with 5 mL of RPMI medium and then maintained at 37 °C in a humidified atmosphere with 5% CO_2 for 18h. The following day, two mixes were prepared: one with 250 μL of opti-MEM (Gibco, USA), and 15 μL of lipofectamine (Invitrogen, USA) and another with 125 μL of opti-MEM, 12 μL of P3000 reagent (Invitrogen, USA), and 6 μg of Ndr 2 plasmid. Then both mixes were combined and incubated at RT, for 15 min. The medium of the cells was removed and replaced with 5 mL of opti-MEM. After incubation, the final mix was added to the cells, drop-by-drop, and incubated at 37 °C / 5% CO_2 for 8 h, after which opti-MEM was changed to RPMI.

In the morning of the next day, puromycin (Sigma, USA) was added to the transfected cells and kept for 30h, in order to select the cells that had successfully incorporated the plasmid of interest. Once the cells reached a confluence of around 70%, we performed a single cell dilution into a 96 multi-well plate to obtain multiple clones that could be further expanded.

Simultaneously, we also conducted a transfection using a GFP plasmid instead of Ndr plasmid in order to assess the transfection efficiency using a fluorescence microscope.

2.1.17 DNA Extraction and Purification

DNA was isolated from BV-2 microglial cells using ethanol precipitation. Briefly, BV-2 microglial cells were lysed at 56 °C for 4 h in a lysis buffer (5 M NaCl, 1 M Tris-HCl pH8, 0.5 M EDTA, 10% SDS) supplemented with 1% proteinase K (Promega, USA). Ice-cold 100% ethanol (2.5 volumes) and glycogen (Invitrogen, USA) were added to the cell lysates, and the solution was incubated at -20 °C for 1 h, centrifuged at 10 000 rpm for 15 min at RT, washed with ice-cold 70% ethanol, and centrifuged again at 14 000 rpm for 15 min. The pellet was air-dried for 10 minutes and then resuspended in 30 µL of DEPC water. DNA concentration was assessed by UV-visible spectroscopy in an automated NanoDrop One Microvolume UV-Vis Spectrophotometer (Thermo Fisher Scientific, USA).

Glycogen was used to facilitate the DNA precipitation obtained from the low number of cells.

2.1.18 Sanger Sequence

Following the extraction and purification of DNA from both WT BV-2 and transfected BV-2 cells, a PCR was performed to amplify the genomic region containing the potential mutation. The forward primer was designed for a sequence located in exon 7, upstream of the potential CRISPR-Cas9-induced mutation site, while the reverse primer was designed to a sequence located in exon 8 (Table 3). All PCR products (540 nucleotides in length) were subjected to electrophoresis on a 2% agarose gel, for validation.

The selected PCR were purified, using the PureLink™ Quick Gel Extraction and PCR Purification Combo Kit (Invitrogen, LT), following the manufacturer`s provided protocol. These purified products were then prepared for sequencing: 5 µL at 5 ng/µL of the purified product was mixed with 5 µL of primers Ndr2 exon 7F at 5 pmol/µL (Table 3), and the resulting mixture was sent to Eurofins for Sanger sequencing analysis.

Table 3 – List of primers used for the different experiments and the respective sequences. All sequences are in 5` – 3` order. Forward (F); Reverse (R); Exon (ex).

Gene	Primer Sequence
Ndr2	(ex13 F) GTTGAGAGGTCCATCCTGCC
	(ex14 R) CTGATTCTAGACCCACGGGC
Ywhaz	(ex34 F) CAGCAAGCATACCAAGAAG
	(ex35 R) TCGTAATAGAACACAGAGAAGT
Ndr2	(ex7 F) GTGACATGATGACATTGCTGATG
	(ex8 R) CCTCACACATAACCCGCCAAGC
U6F	(F) GAGGGCCTATTTCCCATGATTCC

2.1.19 Flow cytometry

Basal conditions:

The day before the experiment, 1 x 10^6 cells were transferred into a 25 cm^3 flask with 6 mL of medium. On the experiment day, the cells were mechanically detached from the bottom of the flask and transferred into a Falcon.

Activation with LPS or HG exposure:

Two days before the experiment, 5 x 10^5 cells were seeded into a 6-multi-well plate. The day before the experiment, the cells were exposed to HG or treated with 100 ng/mL of lipopolysaccharide (LPS) (Sigma-Aldrich, USA) for 24h. To inhibit protein transport from the endoplasmic reticulum to the Golgi complex, which allows the accumulation of cytokines and better detection by flow cytometry, 5µL of Brefeldin A (BD, USA, GolgiPlug™) was added to the culture 4 hours before the end of the 24h incubation period. Following this 4-hour incubation with Brefeldin A, the cells were gently detached from the well's surface and transferred into a Falcon tube.

Staining for flow cytometry:

The cells were centrifuged at 1500 rpm for 5 minutes and resuspended in cell culture medium. Subsequently, 100 µL were resuspended into different flow cytometry tubes, each assigned to different controls and staining conditions essential for the flow cytometry assay. The control conditions include single labeling controls for compensation and unstained cells to adjust parameters on the flow cytometer. The work conditions were categorized into two

tube groups: the first for extracellular labeling without permeabilization (control of permeabilization) and the second for combined extracellular and intracellular labeling with permeabilization. Antibodies for extracellular labeling (CD11b-V500, P2γ12-APC) were added in all tubes, thoroughly mixed, and then incubated for 15 minutes in the dark at room temperature. After incubation, 2 mL of PBS were added, and the tubes were centrifuged at 1500 rpm for 5 minutes.

For tubes in the first category, the supernatant was aspirated and replaced with 200 µL of PBS for flow cytometry reading. For tubes in the second category, 100 µL of Fix and Perm A (Fixation Medium) solution (Invitrogen, USA) was added. The tubes were further incubated for 10 minutes. After incubation, 2 mL of PBS were added, followed by another centrifugation at 1500 rpm for 5 minutes. The supernatant was removed and 100 µL of Fix and Perm B (Permeabilization Medium) solution (Invitrogen, USA) were added along with the intracellular antibodies (TNF-PE, IL-17a-V450), followed by a 20-minute incubation in the dark and at room temperature. Finally, 2 mL of PBS were added, and the tubes were once again subjected to centrifugation at 1500 rpm for 5 minutes, with supernatant removal. This washing step was repeated once more, and lastly, 200 µL of PBS were added to the tubes for flow cytometry reading.

2.2 *In vivo* studies

Ethics statement

Experimental animals were handled in accordance with the guidelines (2010/63/EU) for the use of experimental animals, translated to the Portuguese law in 2013 (Decreto-lei113/2013). In addition, all procedures involving animals were conducted in accordance with the Association for Research in Vision and Ophthalmology (ARVO) Statement for the Use of Animals in Ophthalmic and Vision Research and were approved by Animal Welfare Committee of the Coimbra Institute for Clinical and Biomedical Research (iCBR), Faculty of Medicine, University of Coimbra (ORBEA 9-2022).

2.2.1 Type 1 diabetes induction in C57BL/6J mice

Streptozotocin (STZ) is an antineoplastic agent with a damaging impact on mammalian pancreatic beta cells, and it is frequently used to induce diabetes in animal models [57].

For the experiments, an intraperitoneal (i.p.) daily injection was administered at a dose of 55 mg / kg for males and 75 mg / kg for females mice, 2 months old, over 5 consecutive days. Glycemia was measured at different timepoints by collecting one drop of blood from the tip of the tail. Diabetic mice were selected when their blood glucose levels exceeded 300 mg/dL (Figure 11).

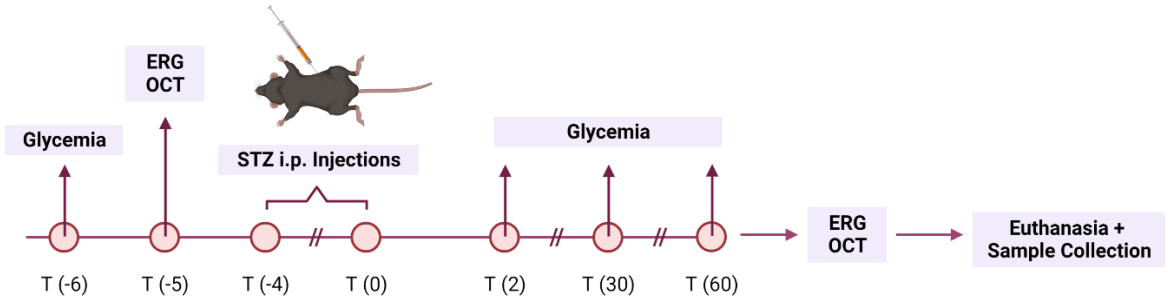

Figure 11 – Schematic timeline of in vivo assays performed in C57BL/6J mice. Timeline of in vivo assays performed in C57BL/6J mice to study the effects of diabetes on the retina. (Created with BioRender.com)

2.2.2 C57BL/6J mice eye dissection

To prepare retinal tissue for analysis, mice were euthanized throughout cervical dislocation. The eyes were then removed, enucleated, and fixed in 4% paraformaldehyde (PFA) in PBS while kept on ice for 15 minutes. Following fixation, the eyes were transferred to a dissection dish filled with PBS and placed under a dissecting microscope. A small incision was carefully made, and a circumferential cut was performed to remove the cornea. The lens was extracted, and the retina was delicately exposed as a white surface covering the inside of the posterior eye cup. Subsequently, the eye cups were washed in PBS and cryoprotected using a 15% sucrose solution. The cryoprotected eye cups were then embedded in OCT in cryomolds and rapidly frozen by immersing the molds in liquid nitrogen. Finally, the frozen blocks were stored at -80 °C and marked with a pen for proper orientation [58].

2.2.3 Mice eye sectioning

The cryostat temperature was adjusted to -23 °C, and the object temperature was set to -22°C. The mold with the embedded eye cups was positioned in a dorso-ventral orientation, and sections were cut at a thickness of 12 µm. Finally, retinal sections were placed on

superfrost microscope slides and stored at -80 °C to preserve the tissue for future analysis [58].

CHAPTER 3 – Results

3.1 Results

In this study, we sought to investigate the effects of HG exposure on microglial cells and specifically the role of NDR kinases in this process. Our object was to mimic the hyperglycemic environment that occurs in diabetes and understand how it impacts the behavior of microglial cells. For that purpose, BV-2 cells were chosen as an established in vitro model to study microglial responses to HG exposure.

3.1.1 Changes observed in BV-2 cultured cells exposed to HG levels are not due to osmotic effects

In this study, we pretend to understand the role of NDR kinases on microglial cells under diabetic retinopahty conditions. To mimic the acute flutuations in glycemia that occur in vivo, we exposed BV-2 cultured cells to shifts from normal levels of glucose (CT) to high levels of glucose (HG) and then back to normal levels. Previous studies have already expose microglial cells to different levels of glucose to evaluate their cytotoxicity [59], [60]. Based on scientific literature, we chose to use a concentration of 30.5 mM of glucose for HG conditions [36], [61]. The concentration of glucose in CT conditions was 5.5 mM. Additionally, we also incubated cells with 25 mM of mannitol (M) along with 5.5 mM of D-glucose already present in cell culture medium, which was used as an osmotic control to ensure that the observed effects from HG exposure were not due to osmotic flutuations. Our results demonstrate that mannitol did not affect the viability of the cells (M: 96.3 ± 21.8 % of control) (Figure 12). Based on our results and the existing literature that shows that this concentration of mannitol does not affect BV-2 cells [36], [59], [61], [62], and to optimize the use of sample material, we decided to not use mannitol as a control for the subsequent set of experiments.

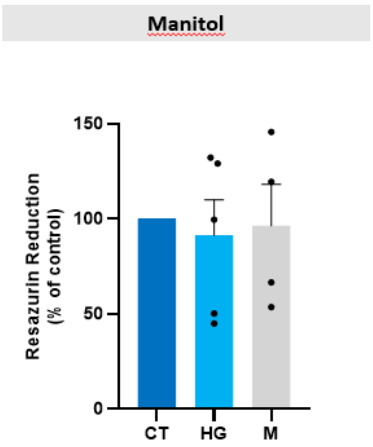

Figure 12 – Increases in the osmolarity of the medium do not induce significant changes in BV-2 cell viability. The viability of BV-2 cells was assessed by resazurin reduction. BV-2 cell cultures were incubated in 5.5 mM glucose (CT), 30.5 mM glucose (HG) or 30.5 mM mannitol (M) for 4h. All the results are expressed as percentage of control ± SEM, and statistical analysis was assessed with one-way ANOVA test.

3.1.2 High glucose exposure alters the NDR1/2 protein expression in BV-2 microglial cells for the 7h assay

To assess if the NDR1/2 protein levels are affected under diabetic conditions, we performed a Western Blot analysis. As illustrated in Figure 13, there was a statistically significant decrease ($p \leq 0.05$) in the expression of NDR1/2 for the 7h HG exposure when compared to CT conditions (CT 7h: 100.0 ± 17.1 %; HG 7h: 81.5 ± 12.2 % of control). For the other assays no statistically significant alteration were detected in these protein levels, but a slight decrease can be observed, particularly in BV-2 cells submitted to the 12h assay (CT 12h: 100.0 ± 8.7 %; HG 12h: 91.3 ± 11.3 % of control), (CT 4h: 100.0 ± 12.2 %; HG 4h: 71.9 ± 8.6 % of control).

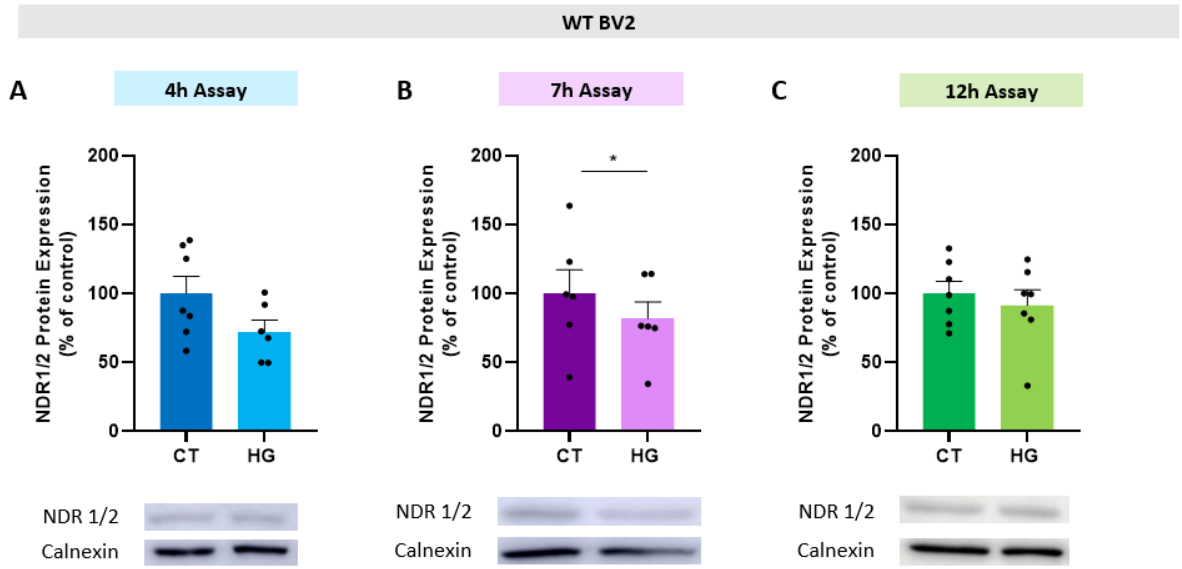

Figure 13 – NDR1/2 protein and expression levels in BV-2 cultured cells. The protein levels of NDR1/2 were evaluated by Western Blot analysis. BV-2 cell cultures were incubated in 5.5 mM glucose (CT) or 30.5 mM glucose (HG) for different timepoints: **(A)** 4h HG assay; **(B)** 7h HG assay; **(C)** two times 4h HG with a break of 4h in between. Representative Western Blots are presented below the graphs. All the results are expressed as percentage of control ± SEM, and statistical analysis was assessed with a student`s t-test after confirmation of a Gaussian distribution; * $p \leq 0.05$: HG compared with CT.

3.1.3 High glucose alters the NDR1/2 protein expression in BV-2 microglial cells

The NDR1/2 protein expression under high glucose conditions was also evaluated through immunocytochemistry. For that, cells were incubated with the Ndr1/2 primary antibody, and the mean fluorescence intensity (MFI) was evaluated and compared with the respective controls. Figure 14 shows that for 7h and 4h exposures there was a decrease in NDR1/2 expression when compared to cells that were only exposed to normal glucose levels. This decrease it is only statistically significant ($p \leq 0.05$) for the 7h incubation (CT 4h: 100.0 ± 19.2 %; HG 4h: 73.1 ± 18.3 % of control) (CT 7h: 100.0 ± 11.9 %; HG 7h: 66.8 ± 15.0 % of control). In contrast, there was an increase ($p \leq 0.01$) in the expression of the NDR1/2 protein in cells submitted to the 12h incubation, (CT 12h: 100.0 ± 7.5 %; HG 12h: 153.4 ± 11.5 % of control). Moreover, we observed that the NDR1/2 localization pattern change between CT and HG condition. In CT condition, NDR1/2 are mostly diffusely localized throughout the cytoplasm, while in HG NDR1/2 are also presented in bright spots near the nuclear membrane (Figure 14 D).

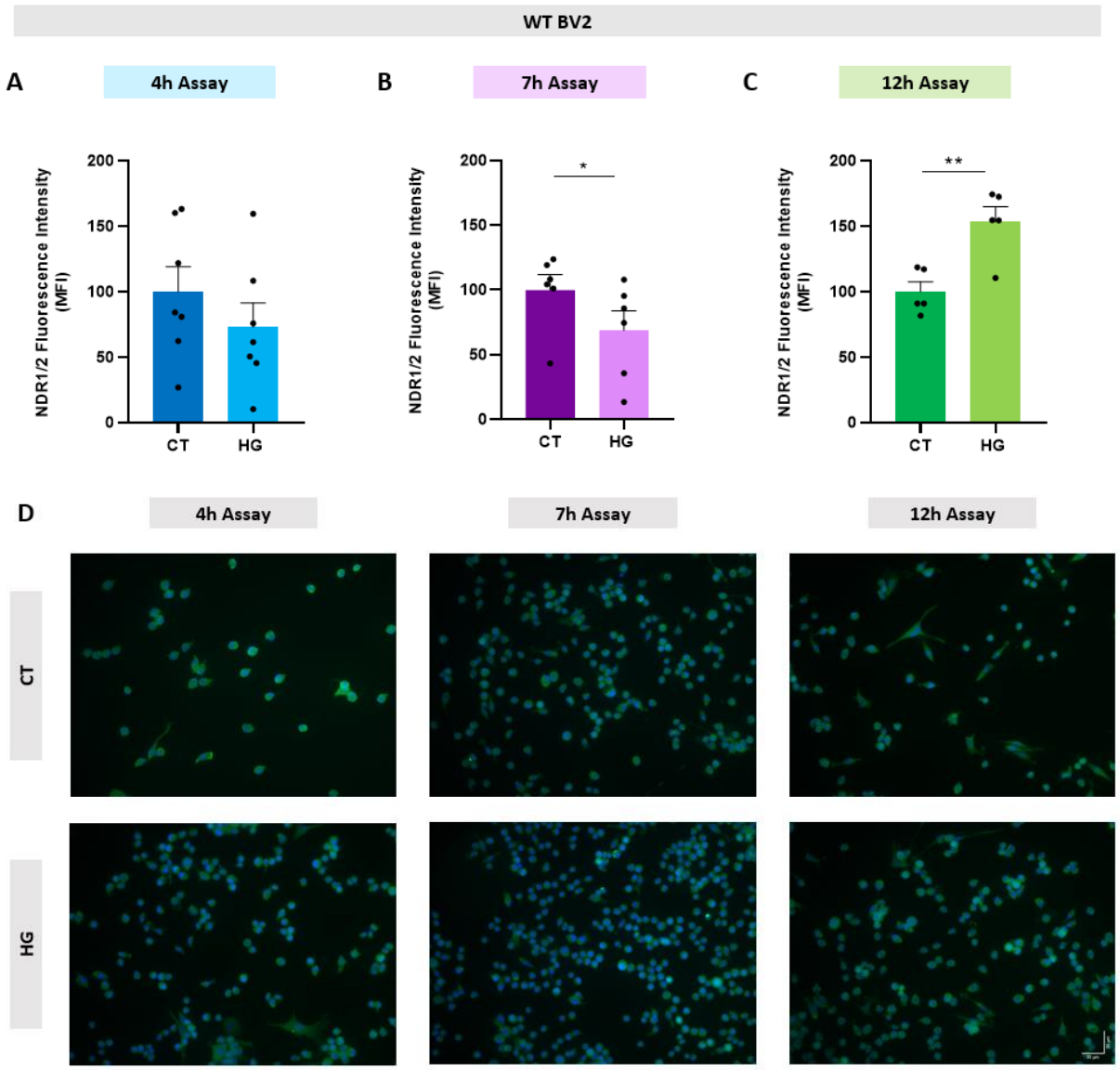

Figure 14 – NDR1/2 protein expression levels in BV-2 cultured cells. The protein levels of NDR1/2 were evaluated by Immunocytochemestry analysis. BV-2 cell cultures were incubated in 5.5 mM glucose (CT) or 30.5 mM glucose (HG) for different timepoints: **(A)** 4h HG assay; **(B)** 7h HG assay; **(C)** two times 4h HG with a break of 4h in between. All the results are expressed as percentage of control ± SEM of the mean of fluorescence intensity (MFI), and statistical analysis was assessed with a student`s t-test after confirmation of a Gaussian distribution; * $p \leq 0.05$; ** $p \leq 0.01$: compared with CT. **(D)** Representative fluorescent images of BV-2 cells stained with Ndr1/2 antibody (green) and the nuclear marker DAPI (blue). For the analysis the background of all images was removed.

3.1.4 High glucose exposure alters the NDR2 mRNA expression in BV-2 microglial cells for the 7h assay

To determine the impact of HG exposure on Ndr2 mRNA levels in BV-2, we conducted a qRT-PCR analysis. As shown in Figure 15, there was a significant decrease ($p \leq 0.05$) in the expression of NDR2 for the 7h HG exposure when compared to CT conditions (HG 7h: 0.5 ± 0.1). Contrarily, for the 4h and 12h incubations, we observed an increase in the Ndr2

mRNA expression compared to the CT, which was nevertheless not statistically significant (HG 4h: 2.2 ± 0.7; HG 12h: 1.5 ± 0.2).

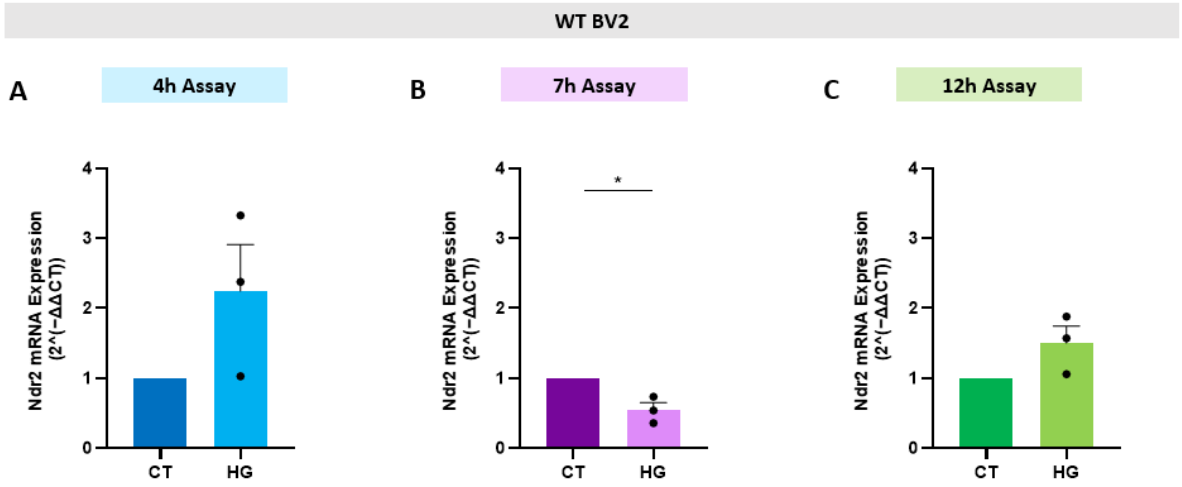

Figure 15 – NDR2 mRNA expression levels in BV-2 cultured cells. The mRNA levels of NDR2 were evaluated by qRT-PCR analysis. BV-2 cell cultures were incubated in 5.5 mM glucose (CT) or 30.5 mM glucose (HG) for different timepoints: **(A)** 4h HG assay; **(B)** 7h HG assay; **(C)** two times 4h HG with a break of 4h in between. All the results are normalized to control ± SEM, and statistical analysis was assessed with a student`s t-test: * p ≤ 0.05: HG compared with CT.

3.1.5 Screening of possible Indels in exon 7 of Ndr2 gene by Sanger Sequencing

In this study, we employed CRISPR-Cas9 technology to perform a Ndr2 knockout (KO) in BV-2 cells. To validate the possible KO obtained by CRISPR/Cas9, we screened 10 clonal population of BV-2 cells transfected with pX459 plasmid containing a sgRNA against the exon 7 of the Ndr2 gene using Sanger sequencing.

The Sanger sequencing results of several clones revealed three distinct alterations in the base pair (bp) sequence between the WT BV-2 cells and the cells transfected using the CRISPR-Cas9 strategy, indicative of a successful gene editing outcome. Considering these results, we chose to work with one clone from two categories that were most likely to generate possible KOs: clone 19 and clone 22 (WT BV-2: 37 bp; Ndr2 KO BV-2 Clone 19: 36 bp; Ndr2 KO BV-2 Clone 22: 40 bp; Figure 16). These variations are known as insertions or deletions (indels), and result in a change in the reading frame of the target gene, causing a frameshift mutation. Consequently, the encoded protein is likely to be altered or truncated, potentially leading to functional changes or loss of function.

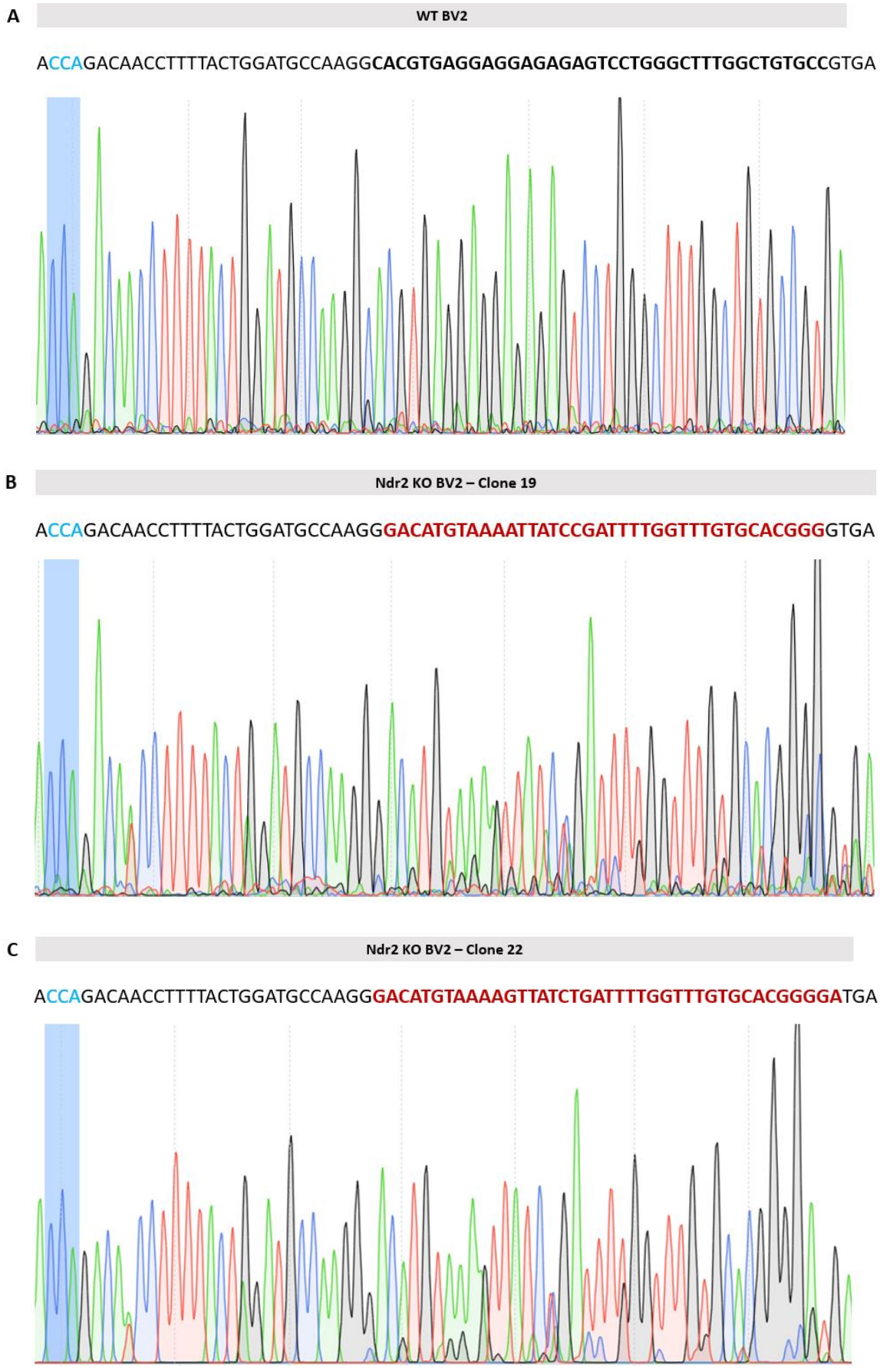

Figure 16 – Sanger Sequencing Results of Ndr2 Gene Editing using CRISPR-Cas9 Strategy. (A) The chromatogram displays the baseline DNA sequence of the Ndr2 gene in WT BV-2 cells. **(B, C)** The chromatogram displays the DNA sequence of BV-2 cells after the CRISPR-Cas9 strategy was applied.

3.1.6 CRISPR-Cas 9 strategy induced a downregulation of the Ndr2 gene

Following Sanger sequencing analysis, we performed two validation assays to confirm that, indeed, we have a disruption of the Ndr2 gene.

Firstly, we assessed the Ndr2 mRNA levels by qRT-PCR in the KO cells to compare with WT BV-2. As we can see in Figure 17 (A), both clones presented a statistically significant decrease ($p \leq 0.001$) in the mRNA levels when compared to the control group (Clone 19: 23.5 ± 4.6 % of control; Clone 22: 26.5 ± 2.9 % of control). Additionally, we performed ICC to evaluate the protein expression of NDR2 in both conditions. For that, cells were incubated with an antibody specific to Ndr2, and the results are expressed in Figure 17 (B). We also observed a decrease in the NDR2 protein levels in both selected clones when compared to WT BV-2 expression (Clone 19: 5.2 % of control; Clone 22: 40.9 % of control).

Since we have amplification signals from qRT-PCR results and NDR2 expression from ICC, we can`t consider that these clones present a real KO of the Ndr2 gene. However, there is a clear downregulation of the Ndr2 gene for both clones, which is bigger for clone 19. Therefore, from now on, these clones will be referred to as Ndr2 downregulated BV-2 cells.

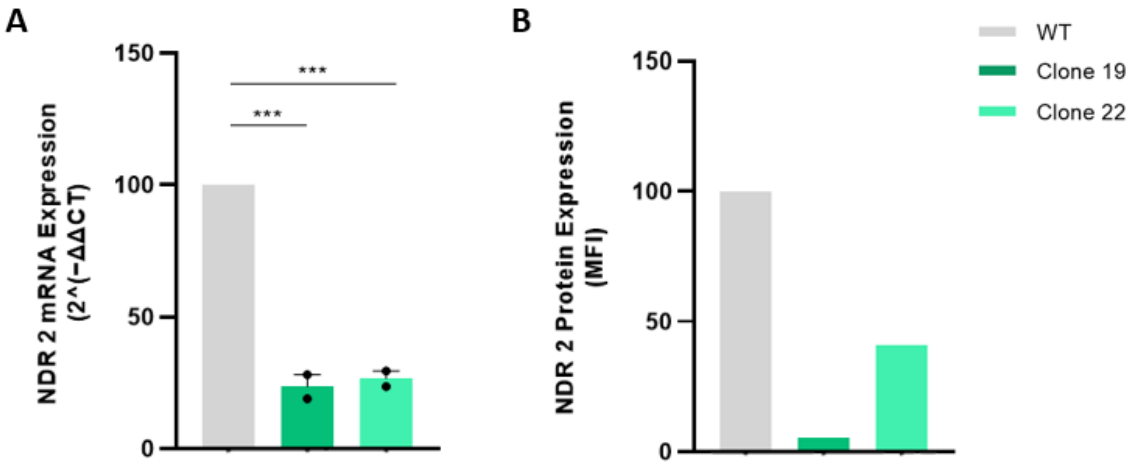

Figure 17 – Validation of Ndr2 KO BV-2 cultured cells by CRISPR/Cas9 strategy. (A) The mRNA levels of NDR2 were evaluated by qRT-PCR in BV-2 (WT) and Ndr2 KO BV-2 (Clone 19 and Clone 22) cultured cells. These results are expressed as percentage of control ± SEM, and statistical analysis was assessed with one-way ANOVA test: *** $p \leq 0.001$. **(B)** The protein levels of NDR2 were evaluated by Immunocytochemistry analysis in BV-2 (WT) and Ndr2 KO BV-2 (Clone 19 e Clone 22) cultured cells. These results are expressed as percentage of control of the mean of fluorescence intensity (MFI).

3.1.7 High glucose levels impact the viability of both WT and Ndr2 downregulated BV-2 cells

To evaluate the effects of Ndr2 downregulation on BV-2 cells, we performed a viability assay based on resazurin reduction. Initially, we evaluated the impact of different timepoints of HG exposure on WT BV-2. The results revealed no difference in cell viability for the 4h incubation when compared to the control condition (HG 4h: 94.4 ± 7.0 % of control) however, there was a significant increase in cell viability for the 7h ($p \leq 0.05$) and 12h exposures ($p \leq 0.01$), (HG 7h: 160.0 ± 19.6 % of control) (HG 12h: 167.1 ± 15.7 % of control), (Figure 18 A-C).

Next, we evaluated the impact of HG on Ndr2 downregulated BV-2 cell viability. For the clone 19, no differences in the resazurin reduction were observed for the 4h and the 7h incubations (Clone 19 – HG 4h: 101.7 ± 37.3 % of control) (Clone 19 – HG 7h: 106.9 ± 25.5 % of control). For the 12h incubation, a decrease in viability was observed when compared to the control, although it did not reach statistical significance (Clone 19 – HG 12h: 79.0 ± 12.7 % of control) (Figure 18 D-F). For the clone 22, no differences were observed in the 12h exposure (Clone 22 – HG 12h: 97.5 ± 9.4 % of control), while a decrease was observed in the other incubations, with statistical significance ($p \leq 0.01$) only reached for the 4h HG exposure (Clone 22 – HG 4h: 56.6 ± 5.5 % of control) (Clone 22 – HG 7h: 83.4 ± 8.6 % of control), (Figure 18 G-I).

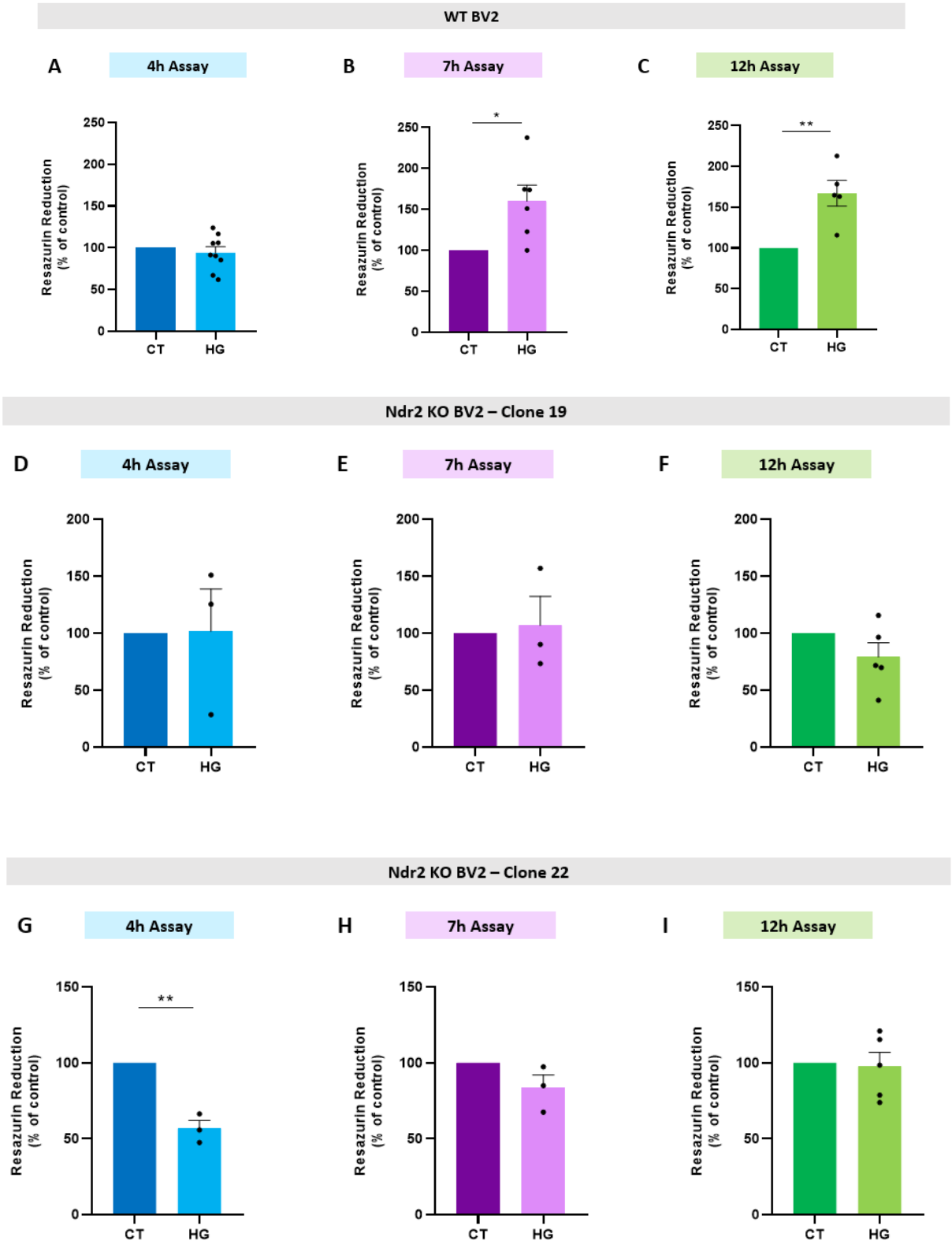

Figure 18 – High glucose exposure affects BV-2 cells viability. WT BV-2 **(A, B, C)** and Ndr2 downregulated BV-2 **(D, E, F, G, H, I)** cell cultures were incubated in 5.5 mM glucose (CT) or 30.5 mM glucose (HG) for different timepoints: **(A, D, G)** 4h HG assay; **(B, E, H)** 7h HG assay; **(C, F, I)** two times 4h HG with a break of 4h in between. All the results are expressed as percentage of control ± SEM, and statistical analysis was assessed with a student`s t-test after confirmation of a Gaussian distribution; * $p \leq 0.05$, ** $p \leq 0.01$: HG compared with CT.

3.1.8 The phagocytic activity of WT and Ndr2 downregulated BV-2 cells is affected by exposure to high glucose conditions

WT BV-2 and Ndr2 downregulated BV-2 cultured cells were treated with HG for different timepoints and then incubated with fluorescent beads to assess the phagocytic activity (Figure 19). Beads uptake by WT BV-2 cells increased after 4h HG exposure, with statistical significance ($p \leq 0.05$), (CT 4h: 55.7 ± 13.5 %; HG 4h: 137.3 ± 20.9 %). Contrarily, for the 12h incubation there was a significant decrease ($p \leq 0.001$) in the phagocytic ability after HG exposure (CT 12h: 157.4 ± 4.0 %; HG 12h: 101.3 ± 11.5 %). For the 7h exposure no significant changes were observed (CT 7h: 79.8 ± 14.8 %; HG 7h: 110.2 ± 11.6 %).

In contrast, incubation of clone 19 BV-2 cells with HG media induced a decrease in phagocytosis for the 4h and 7h incubations when comparing CT with HG conditions, although not statistically significant (Clone 19 – CT 4h: 65.7 ± 2.0 %; HG 4h: 44.9 ± 1.6 %) (Clone 19 – CT 7h: 85.1 ± 22.7 %; HG 7h: 47.6 ± 3.3 %). No alterations were observed for the 12h exposure (Clone 19 – CT 12h: 46.4 ± 19.0 %; HG 12h: 55.2 ± 3.4 %). In the case of clone 22, results showed a not significant decrease in phagocytosis, when compared to control, for the 4h HG exposure (Clone 22 – CT 4h: 115.9 ± 30.5 %; HG 4h: 81.4 ± 27.0 %). No alterations were observed for the 7h and 12h HG exposures (Clone 22 – CT 7h: 81.2 ± 17.8 %; HG 7h: 87.1 ± 18.7 %) (Clone 22 – CT 12h: 100.8 ± 12.1 %; HG 12h: 95.7 ± 15.8 %).

Upon comparing all the results within the CT conditions of all different cell groups, we observed that no differences were identified between WT BV-2 and clone 19 for the 4h and 7h incubations. However, a decrease was evident ($p \leq 0.001$) for the 12h assay when comparing the CT of WT BV-2 with the CT of clone 19. For clone 22, under CT conditions, no differences were found for the 7h exposure when compared to CT BV-2. There was a non-significant increase for the 4h and a significant decrease for the 12h incubation ($p \leq 0.05$).

Finally, within HG conditions, there was consistently a decrease for all the timepoints when comparing WT BV-2 and clone 19, although only the 4h assay reached statistical significance. Between WT BV-2 and clone 22 there was a non-significant decrease for the 4h incubation, and no differences were observed for the other assays (Figure 20).

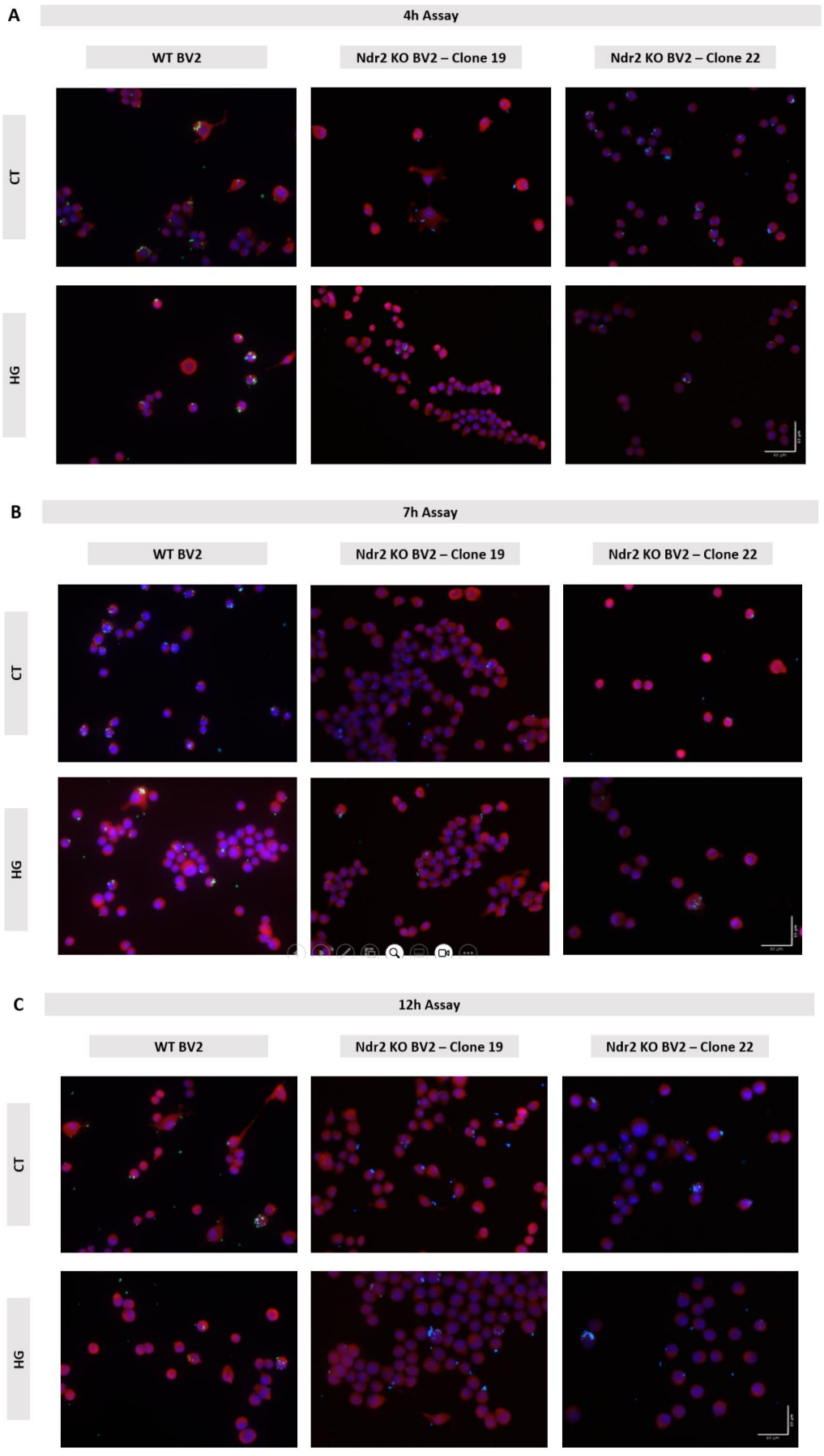

Figure 19 - Representative fluorescent images of phagocytic activity. WT BV-2 (WT) and Ndr2 downregulated BV-2 (Clone 19 and Clone 22) cell cultures were incubated in 5.5 mM glucose (CT) or 30.5 mM glucose (HG) for different

timepoints: **(A)** 4h assay; **(B)** 7h assay; **(C)** 12h assay. Fluorescent beads (green) where used to assess the phagocytic activity and cells were stained with phalloidin (red) and the nuclear marker DAPI (blue). Scale bar: 50 µm x 50 µm.

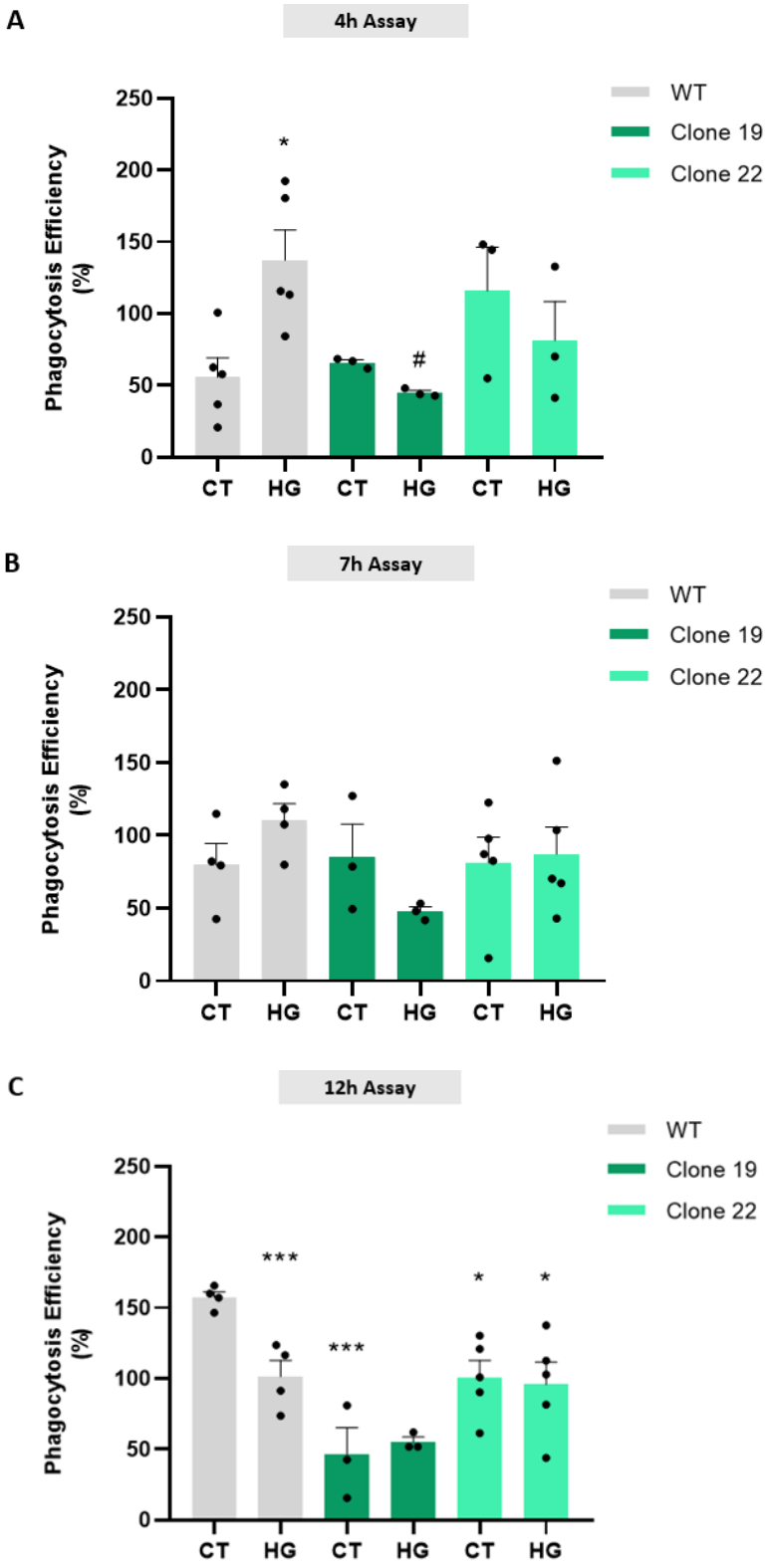

Figure 20 – Phagocytic efficiency of BV-2 cultured cells. WT BV-2 (WT) and Ndr2 downregulated BV-2 (Clone 19 and Clone 22) cell cultures were incubated in 5.5 mM glucose (CT) or 30.5 mM glucose (HG) for different timepoints: **(A)**

4h assay; **(B)** 7h assay; **(C)** 12h assay. All the results are presented as the mean ± SEM, and statistical analysis was assessed with one-way ANOVA test after confirmation of a Gaussian distribution; * $p \leq 0.05$, *** $p \leq 0.001$: compared with WT CT; # $p \leq 0.05$, compared with WT HG.

3.1.9 Ndr2 downregulation and exposure to HG and LPS induce expression of IL-17a and TNF-α

The flow cytometry findings are preliminary results obtained in collaboration with Dr. Paulo Santos of the Immunology and Oncology Laboratory at the Institute of Immunology. In this study, both WT BV-2 cells and Ndr2 downregulated BV-2 clone 19 were subjected to either HG or LPS exposure for 24 hours. For the analysis, CD11b-V500 and P2y12-APC positive cells were selected, which correspond to microglial cells, and then the expression of IL-17a and TNF-α was evaluated. As we can see in Figure 21 in the case of WT BV-2 cells, HG promoted the expression of IL-17a and TNF- α, when compared to the control condition. Similarly, Ndr2 downregulation leads to increased expression of IL-17a and TNF-α to similar levels as LPS, and exposure to HG does not alter their expression levels in comparison to the control. This pattern is consistently observed in response to LPS exposure as well.

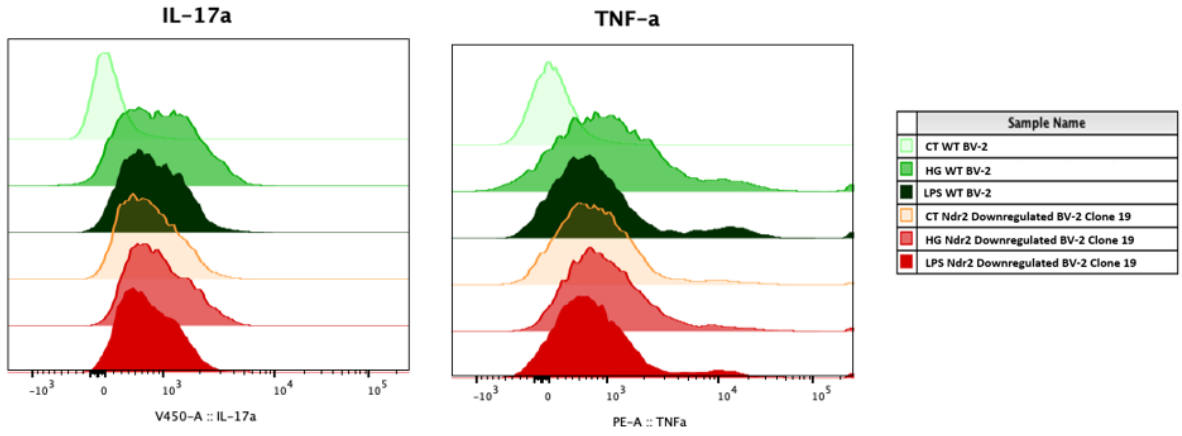

Figure 21 – Expression of IL-17a and TNF-α in BV-2 cultured cells. The IL-17a and TNF-α levels were evaluated by Flow Cytometry analysis. BV-2 cell cultures were incubated in 5.5 mM glucose (CT), 30.5 mM glucose (HG) or 100 ng/mL LPS (LPS) for 24h.

3.1.10 The migration rate of WT BV-2 and Ndr2 downregulated BV-2 cells is affected by high glucose condition

The migration rate of WT BV-2 and Ndr2 downregulated BV-2 cultured cells after 4h of HG exposure was evaluated by the scratch assay, and the results are expressed in Figure 22.

For all the groups, there was a non-significant decrease when comparing the CT group with HG conditions within each group (WT BV-2 CT 4h: 663.8 ± 216.4 %; WT BV-2 HG 4h: 379.4 ± 122.1 %) (Clone 19 – CT 4h: 234.4 ± 14.6 %; HG 4h: 170.4 ± 41.3 %) (Clone 22 – CT 4h: 376.8 ± 38.0 %; HG 4h: 267.5 ± 18.6 %). Additionally, WT BV-2 cells exhibited an increased capacity for migration in both CT and HG conditions when compared to the different clones. Indeed, the migration rate of the WT in HG is similar to the migration rate of the clones 19 and 22 in CT while the migration rate of the clones 19 and 22 in HG is even lower. Among the Ndr2 downregulated BV-2 cells, clone 19 showed the lowest migration rate.

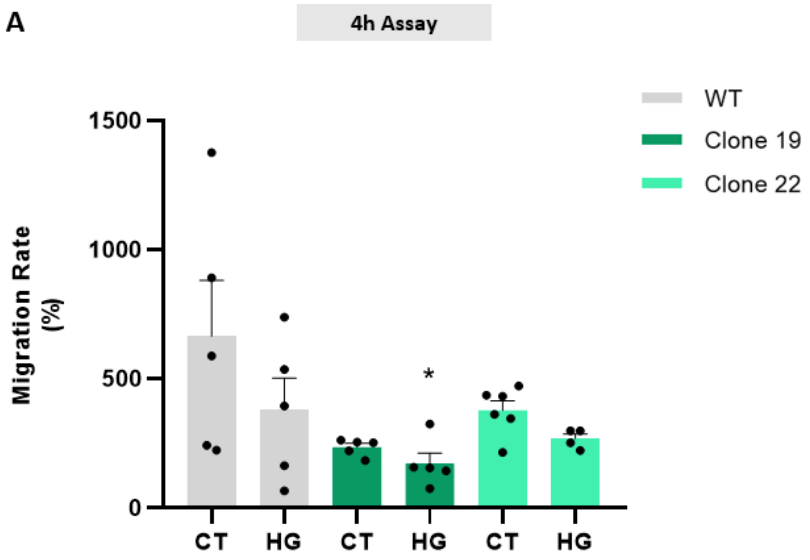

Figure 22 – Migration rate of BV-2 cultured cells. WT BV-2 (WT) and Ndr2 downregulated BV-2 (Clone 19 and Clone 22) cell cultures were incubated in 5.5 mM glucose (CT) or 30.5 mM glucose (HG) for 4h. All the results are presented as the mean ± SEM, and statistical analysis was assessed with one-way ANOVA test after confirmation of a Gaussian distribution; * $p \leq 0.05$, compared with WT HG.

3.1.11 Microglia distribution is altered in retinas of STZ-induced diabetic mice

Diabetes triggers microglial cell activation, and existing literature suggests that activated microglia migrate from the inner to the outer layers of the retina [63]. To assess differences

in microglial cell localization between non-diabetic mice (CT) and diabetic mice (STZ), immunostaining using the Iba1 antibody, a specific marker for microglial cells, was performed. As expressed in Figure 23, the predominant distribution of microglial cells in control mice was observed in the IPL. However, In STZ-induced diabetic mice, a clear migration of microglial cells from IPL to OPL was evident.

Although the findings regarding the migration of activated microglial cells in response to STZ-induced diabetes are not novel, they serve as a crucial foundation for future investigations. In particular, it will be essential to conduct a comparative analysis with the Ndr2 KO mouse model.

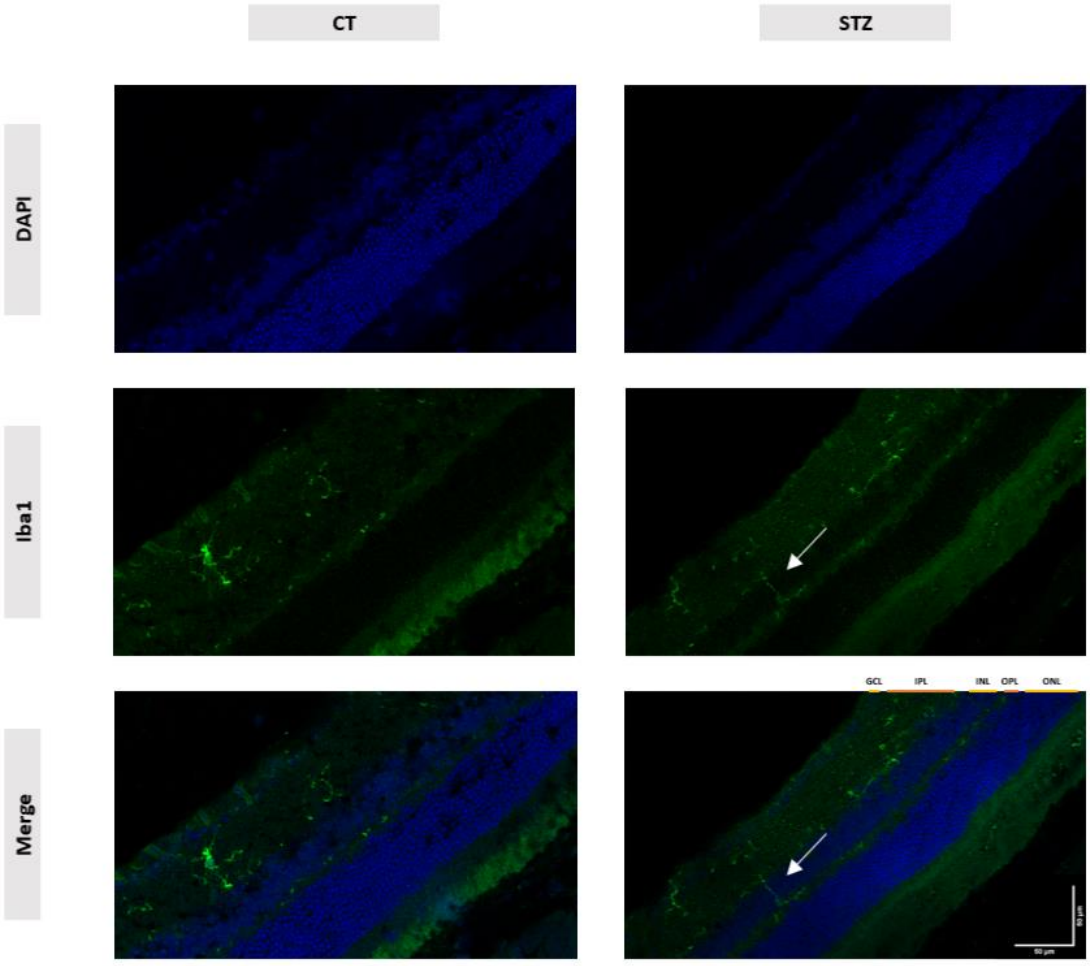

Figure 23 – Representative fluorescent and confocal images of mice retinal microglial cells. Non-diabetic (CT) and STZ-induced diabetic mice`s (4 months old) retinal sections were stained with Iba1 antibody (green) and the nuclear marker DAPI (blue). Activated microglia translocation from the inner plexiform layer (IPL) to the outer plexiform layer (OPL) (white arrow). ONL – outer nuclear layer; OPL – outer plexiform layer; INL – inner nuclear layer; IPL – inner plexiform layer; GCL – ganglion cell layer. Scale bar: 50 µm x 50 µm.

3.1.12 Ndr2 localization is altered in STZ-induced diabetic mice

To assess differences in the retinal distribution of Ndr2 between non-diabetic mice (CT) and diabetic mice (STZ), we conducted immunostaining using the Ndr2 antibody. As expressed in Figure 24, Ndr2 seems to be present across all layers of the retina, from ONL to IPL, in non-diabetic mice, with a more preeminent expression in the inner segment of the photoreceptors (IS) and in the synapse-rich regions OPL and IPL. However, in STZ-induced diabetic mice, the expression of Ndr2 was notably confined to in the inner segment of the photoreceptors and the IPL, with no observable presence in the other retinal layers.

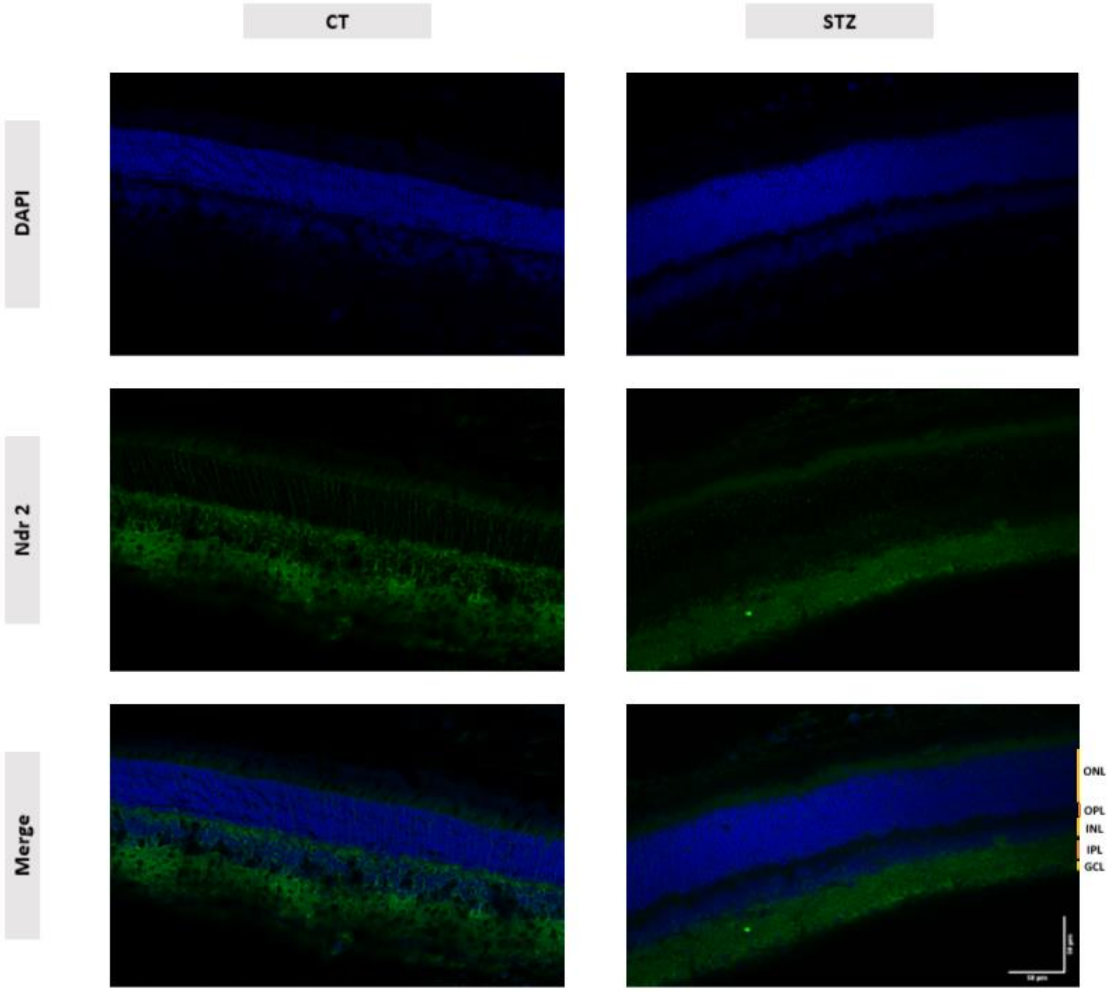

Figure 24 – Representative fluorescent and confocal images of mice retinal sections. Non-diabetic (CT) and STZ-induced diabetic mice (4 months old) retinal sections were stained with Ndr2 antibody (green) and the nuclear marker DAPI (blue). ONL – outer nuclear layer; OPL – outer plexiform layer; INL – inner nuclear layer; IPL – inner plexiform layer; GCL – ganglion cell layer. Scale bar: 50 µm x 50 µm.

3.1.13 Ndr2 mRNA levels are not affected in retinal cells of STZ-induced diabetic mice

The RNA of the retina of CT and STZ-induced diabetic mice was extracted to evaluate the impact of diabetes on Ndr2. For that, we conducted a qRT-PCR analysis, and as shown in Figure 25, no changes were observed when compared to the control group (STZ: 1.6 ± 0.4). Nevertheless, a tendency towards increased Ndr2 mRNA levels can be observed in the diabetic mice. These are preliminary results obtained from a small number of animals (n=2 CT and n=3 STZ) and would need to be repeated with a lagger number of samples.

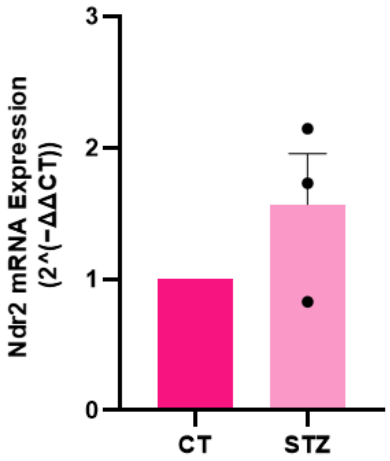

Figure 25 – NDR2 mRNA expression levels in the retina of STZ-induced diabetic mice. The NDR2 mRNA levels of CT and STZ-induced diabetic mice (4 months old) were evaluated by qRT-PCR analysis. The results are normalized to control ± SEM (n=2 control retinas and n=3 STZ retinas).

CHAPTER 4 – Discussion

4.1 Discussion

This study presents, for the first time, novel insights regarding the response of NDR kinases within microglia when exposed to acute high glucose conditions.

It is known that hyperglycemic environments lead to alterations in the cellular metabolism and potentially trigger specific signaling pathways, such as the Hippo pathway, which may influence the expression and stability of NDR kinases [31], [43]. Our findings reveal a statistically significant reduction in NDR1/2 protein expression in BV-2 microglial cells incubated with HG for 7h, when compared to the control. This suggests that prolonged exposure to HG levels can lead to a downregulation of the tumor suppressor NDR1/2 expression in microglial cells, possibly due to cellular stress or altered signaling pathways, leading to the regulation of cell proliferation and/or cell survival. Interestingly, for the 12h assay, where cells are exposed two times 4h to HG with a 4h break with NG in between, there was a statistically significant increase in NDR1/2 protein expression, suggesting a dynamic response to the alternating glucose environment. These results lead us to hypothesize that during the 4h break between HG exposures, the cells might activate compensatory mechanisms to reduce the negative effects of HG-induced stress. However, during longer exposure times (7h), these compensatory mechanisms may no longer be activated. Notably, despite a tendency to decrease, no alterations were observed for the 4h incubation, indicating that may not be enough time to trigger significant changes in NDR1/2 protein expression. The choice of using an antibody that recognizes both NDR1/2 kinases in the protein quantification studies was driven by the fact that NDR1 and NDR2 kinases share a substantial protein sequence similarity of around 90% [41]. Furthermore, at the time this part of the study was carried out, we didn't have a commercially available antibody specific for Ndr2, our main kinase of interest. In terms of localization, we observed that in CT conditions, NDR1/2 are mostly diffusely localized throughout the cytoplasm, while in HG conditions, NDR1/2 are also present near the perinuclear areas or close to the plasma membrane. A similar pattern of expression was observed when we evaluated the Ndr2 mRNA levels in microglial cells after 7h or two time 4h of HG. Our results demonstrated that for the 7h HG exposure, there is a decrease in the Ndr2 mRNA levels, but for the 12h assay, there is a tendency, not statistically significant, for an increased expression. This supports the idea that the 4h break between HG exposures may possibly lead to the activation of compensatory mechanisms. On the other hand, when cells are exposed to HG for 7h there is a decrease in expression, probably because the extended time of exposure may compromise or inhibit the ability and efficiency of the cells to mount compensatory

responses. During shorter periods (4h assay) or intermittent incubations (12h assay), cells might have an opportunity to recover and initiate compensatory mechanisms.

To specifically investigate the role of Ndr2 kinase in microglial responses to HG conditions, we generated Ndr2 KO in BV-2 cells using the gene-editing method CRISPR-Cas9. We performed a lipofectamine transfection to introduce a plasmid coding for the cas9 gene as well as for the sgRNA targeting exon 7 of the Ndr2 gene. The results indicated that nearly all of the 10 clones submitted for sequencing exhibited mutations in the Ndr2 gene, each presenting an insertion/deletion (indel) in the region near the PAM sequence. This homogeneity among the clones could be explained by the fact that we let the mixed population of cells grow again after the puromycin selection and before the single cell dilution, thus amplifying certain indels. Different clonal populations of KO cells were validated through qRT-PCR and ICC, using a commercially available antibody specific for Ndr2, which revealed a downregulation instead of a complete absence of Ndr2. Two distinct clones, labeled as clone 19 and clone 22, were employed in our study, and results indicated that clone 19 exhibited a lower level of Ndr2 expression compared to clone 22. These results could be explained by either the presence of WT cells in our KO population due to a or the use of a polyclonal antibody against NDR2. Indeed, this commercially available Ndr2-specific polyclonal antibody was raised against an epitope located between the amino acids 380 and 460 (Ndr2 C-term.) that partially overlaps with the Ndr1 kinase. This could also explain the increased staining in HG, as NDR1 is known to be upregulated when NDR2 is absent.

Viability studies hold significance because cell viability is closely linked to cellular functions. A decrease in viability might indicate compromised cellular functions, such as altered metabolism, impaired signaling, or a reduced ability to respond to stress. In the literature, microglial cells are usually incubated with HG for longer periods of time, such as 24h, 48h, 72h, and 7 days [60], [61]. In our study, we pretend to mimic what happens after the acute variation of glycemic experienced by diabetic patients after a meal or after insulin administration. Research conducted with BV-2 cells revealed that 48h exposure to HG concentrations of 100 mM or higher resulted in a reduction in cell viability [64]. There are also some studies using another type of cells, such as retinal neuronal cells and retinal pigment epithelium cells, that have demonstrated that during 24h or 48h and 7 days, respectively, HG levels induced a decrease in cellular viability [62], [65], [66]. Our findings revealed that there is an increase in WT BV-2 viability for the 7h and 12h assay, when compared to control conditions. High glucose concentrations might provide additional energy substrates that promote cell metabolism and proliferation, therefore promoting a cell

viability increase. While cells may initially benefit from increased glucose availability, extended exposure to HG can lead to oxidative stress, apoptosis, and the accumulation of damaging products, all of which can ultimately result in decreased cell viability.

Knowing that Ndr2 is a tumor suppressor and that it affects cell growth and survival [67], viability becomes a critical and important assay to perform. In the case of Ndr2 downregulated BV-2 cells, clone 19 didn't present any differences between the control and HG conditions after all timepoints of incubation, and the same happened for clone 22 for the 7h and 12h assays. These results suggest that Ndr2 downregulated BV-2 cells don't have the ability to use the increased glucose as an energy source. Based on literature, NDR kinases are key effectors of the Hippo pathway that regulates cell proliferation, differentiation, and apoptosis [40]. The downregulation of Ndr2 can possibly disturb this pathway, and glucose, instead of being a source of energy, becomes a source of stress. This conclusion is supported by previous studies showing that Ndr2 kinase is regulated by oxidative stress and can prevent oxidative stress-induced cell death [68]. In this study, a direct comparison of the viability between WT BV-2 and Ndr2 downregulated BV-2 was not possible because the experiments were conducted on different days. The viability of WT BV-2 was assessed prior to the generation of the KO cell line. However, a comparative analysis between these two cell types is planned for future research.

Phagocytosis is one of the main functions of microglial cells, as these cells play a vital role in the surveillance of the surrounding environment. They are responsible for the removal of cellular debris, apoptotic cells, and invading microorganisms [69]. The observed results reveal intriguing variations in the phagocytic activity of BV-2 cells under different HG exposure timepoints. In the case of a 4h HG exposure, an increase in phagocytic activity was observed. This could potentially be attributed to an initial surge of cellular response triggered by the abrupt change in glucose environment. However, for the 7h HG exposure, no significant changes in phagocytosis were evident, possibly indicating a level of adaptation reached by microglial cells within this time frame. Interestingly, when BV-2 cells were exposed to two cycles of 4h HG exposure with a 4h break under normal glucose conditions (12h assay), a noteworthy decrease in phagocytic activity was noted. This outcome could be the result of a cumulative effect, where repeated exposure to HG might have led to some level of cellular stress or altered metabolic activity, resulting in a reduced phagocytic response, or it could be the result of an adaptative response to a repetitive stress (two HG exposures).

Phagocytosis is a complex process that involves the rearrangement of the cells` cytoskeleton and membrane components to engulf and internalize particles [70]. Ndr2 kinase, being

involved in cytoskeletal organization and cell morphology, can influence the efficiency of these processes [71]. The phagocytic activity of Ndr2 downregulated BV-2 cells is inherently less responsive to changes in glucose concentrations since no changes were observed between CT and HG conditions for both clones and for all the different incubation times. This reduced responsiveness could be attributed to the downregulation of Ndr2, which may influence the signaling pathways and cellular mechanisms that modulate phagocytosis. The generation of Ndr2 KO cells allows us to understand the cellular behavior differences between WT and Ndr2 downregulated BV-2 cells, which could have implications for the pathophysiology of the disease. Our results shown that in the 12h assay, when comparing WT with Ndr2 KO BV-2, a reduction was observed between control conditions. However, this reduction cannot be exclusively attributed to the downregulation of Ndr2, as no differences were observed for other assays. One possible explanation could be that the control cells in the 12h assay go through four medium changes, and even though the new medium is always the same, the repeated changes may subject the cells to some levels of stress, which may be amplified for the downregulated cells, impairing the phagocytic activity. Among HG conditions, changes were only observed for the 4h HG incubation between WT BV-2 and Ndr2 downregulated BV-2 clone 19. Nevertheless, a tendency towards reduced phagocytosis is apparent for the remaining timepoints. To address the veracity of these results, more replicates of the experiment (n) are needed. Moreover, it's noteworthy that additional investigations are necessary since alternative signaling pathways or other molecular factors might play a more significant role in regulating phagocytosis in Ndr2 downregulated BV-2 cells.

Retinal microglial cells, in response to pathological stimulation, are capable of changing their morphology and migrating within the retinal tissue, contributing to their crucial role in maintaining retinal homeostasis and responding to injury [72]. Hyperglycemia could potentially influence cellular behaviors, as exposure to HG conditions leads to a tendency for reduced migratory activity in both WT and Ndr2 downregulated BV-2 cells. This migratory capacity is also affected by Ndr2 downregulation since a tendency for decrease is observed when compared to WT cells. This is supported by the fact that NDR1/2 is known to play important roles in thymocyte egress and migration [40].

Diabetes can activate microglia and trigger their migration to areas of injury as a response to retinal inflammation and stress caused by hyperglycemia. Here we evaluated the distribution and localization of microglial cells in STZ-induced diabetic mice as a control for future work with Ndr2 KO mice. Previous research by Kangjia and colleagues revealed that microglia in 4-month-old non-diabetic mice are present in the IPL and OPL, whereas in diabetic mice

induced by STZ, microglial cells were identified in the ONL [63]. Another study involving 1-week-old STZ-induced diabetic rats demonstrated that microglia migrate from the IPL to the OPL in response to diabetic conditions [73]. This last one is in accordance with our findings. Our research using 4-month-old mice revealed the presence of microglial cells within the IPL of control mice. In 4-month-old STZ-induced diabetic mice, we observed that microglia migrate from the IPL to the OPL. Even though our animals are 4 months old, they have only been diabetic for 2 months, considered mid-phase diabetes. Possibly, if we analyzed mice with more than 2 months of diabetes, we might observe microglia in the ONL, but for that, further research is required.

Ndr2 localization was also evaluated in 4-month-old non-diabetic and STZ-induced diabetic mice using a commercially available Ndr2-specific polyclonal antibody raised against an epitope located between the amino acids 380 and 460 (Ndr2 C-term.). This region possesses one of the two unique Ndr2-specific peptide antigens corresponding to amino acids 421–434, previously used to generate an Ndr2-specific antibody. Based on the literature, Ndr2 kinase is localized in the inner segments of the photoreceptors (IS), as well as in the synapse-rich inner (IPL) and outer plexiform layers (OPL) [74]. Our findings agree with this statement. We have found that Ndr2 in non-diabetic mice is present in all retinal layers, from ONL to IPL, especially in the IS, IPL, and OPL. However, when mice are injected with STZ, Ndr2 localization changes and the expression is confined to the IS and IPL. In conclusion, diabetes seems to decrease the expression of Ndr2 in the GCL and in the OPL, a layer rich in synapses between the photoreceptors and horizontal and bipolar cells. In other words, NDR kinases may have a role in modulating synaptic function that is impacted by hyperglycemic environments. Changes in synaptic activity could influence the processing of visual information within the retina. Altered synaptic function may affect how signals from photoreceptors are relayed to higher-order retinal cells and eventually transmitted to the brain. Indeed, Léger and colleagues have already demonstrated that Ndr2 deletion decreases the expression of genes involved in synapse function and modulation and promotes a decrease in amacrine cell differentiation [74].

IL-17a and TNF-α are pro-inflammatory cytokines produced by immune cells, including microglia, as part of the immune response and play a role in recruiting and activating immune cells to fight potential threats or respond to tissue damage [75], [76]. Their expression levels can provide insights into the degree of inflammation within microglial cells, which is essential for understanding the immune response in conditions like diabetic retinopathy. Several studies have previously evaluated the expression of TNF-α under HG conditions. Increased

levels of TNF- α have been detected in rat microglia after at least 6h of HG exposure [77]. Furthermore, the mRNA levels of this pro-inflammatory cytokine have shown an increase in BV-2 cells treated with HG [78]. TNF-α has been found in the retinas of STZ-induced diabetic mice [79] and in the serum of DR patients [80]. Regarding IL-17a, there is relatively limited research available, but a study has concluded that diabetes leads to an elevated retinal expression of IL-17a, suggesting the potential involvement of this cytokine in DR [81]. Our results have demonstrated that within WT BV-2 cells there was an upregulation of IL-17a and TNF-α for HG and LPS conditions, which validates our model. Hyperglycemia is known to trigger an inflammatory response in various cell types, including microglial cells. When exposed to HG levels or LPS, microglia may perceive this as a pathological stimulus, triggering an immune response. This response could be a protective mechanism to maintain tissue homeostasis. Ndr2 downregulation in CT conditions also induced an upregulation of IL-17a and TNF-α. The levels of expression of those cytokines are the same as observed for WT BV-2 exposed to HG or LPS and are also the same observed for Ndr2 downregulated BV-2 exposed to HG or LPS. Since expression of IL-17a and TNF-α is observed for both CT and HG conditions, Ndr2 potentially play a role in modulating immune responses and its downregulation can lead to an enhanced immune response characterized by increased cytokine production. This aligns with findings from studies conducted in macrophages, which have demonstrated that Ndr2 functions as an inhibitor of IL-17 and NF-kB signaling (TNF-α) [82]. These preliminary results corroborate our hypothesis that Ndr2 downregulated microglial cells will exhibit a higher expression of IL-17 and TNF-α, which is regulated by NF-kB signaling, and will have more difficulty adapting to an environmental stress like HG exposure. Ndr2 deprived cells lose the ability to respond to a stress stimulus as they are already in an activated state and producing higher levels of cytokines. These data are also in concordance with previous data from Léger and colleges that have established that Ndr2 deletion in mice results in deregulation of stress- and inflammation-related gene expression in the retina. [83] Additionally, it leads to the migration of Iba1-positive cells (microglia) towards the outer retina and an upregulation in retinal expression of the activated NF-kB p65 subunit (p-p65) in 1-month-old animals (preliminary data not presented in this thesis).

Collectively, our discoveries indicate that hyperglycemic environments impact Ndr2 kinase, which in turn has an impact on retinal microglial cells. The employment of a Ndr2 KO in BV-2 cells has enabled us to gain insights into the function of Ndr2 kinase in microglial responses under HG conditions, suggesting that the downregulation of Ndr2 causes an upregulation of IL-17 and NF-kB signaling from the microglial cells. Moreover, the deletion of Ndr2 leads to

an upregulation of gene expression related to stress and inflammation within the retina, including components of the NF-kB signaling pathway. Therefore, NDR2 kinase is an important regulator of the inflammatory response mediated by retinal microglia cells within the context of diabetic retinopathy. This study also suggests that Ndr2 plays a role in retinal functions, particularly in synaptic processes and the processing of visual information. These are the preliminary results, and further research is needed to elucidate the precise mechanisms underlying the role of Ndr in response to HG conditions and uncover the specific pathways and interactions involved.

CHAPTER 5 – Conclusion

5.1 Conclusion

Diabetic retinopathy is a severe complication of diabetes and a leading cause of visual impairment worldwide. It is well established that hyperglycemia plays a critical role in the pathogenesis of DR, triggering an array of cellular responses within the retina. However, the role of NDR kinases, particullarly NDR2, in the context of DR remains largely unexplored. Based on that, this work started with the purpose of deciphering the functions of NDR kinases in microglial cells after acute HG exposure. The main conclusions of this study were:

- Decreased protein levels of NDR1/2 were observed for WT BV-2 cells exposed to the 7h assay, while an increase in protein levels of NDR1/2 was noted for cells subjected to the 12-hour assay.
- Ndr2 mRNA levels exhibited a reduction in WT BV-2 cells following 7h exposure to HG and a tendency towards increased expression in cells exposed to the 12h assay.
- Enhanced cell viability was evident in BV-2 cells following 7h and 12h assay HG exposure.
- Ndr2 downregulated BV-2 cells demonstrated an impaired ability to utilize increased glucose as an energy source.
- Increased phagocytosis for WT BV-2 incubated with HG for 4h, yet decreased in WT BV-2 cells submitted to the 12h assay.
- The phagocytic activity of Ndr2 downregulated BV-2 cells displayed reduced responsiveness to changes in glucose.
- In diabetic STZ-induced mice, retinal microglia exhibited a shift from the inner plexiform layer (IPL) to the outer plexiform layer (OPL).
- Diabetic conditions appeared to decrease the expression of NDR2 in the OPL in STZ-induced diabetic mice, with localization confined to the IS and the IPL.
- Both HG conditions and Ndr2 downregulation correlated with the upregulation of inflammatory cytokines IL-17a and TNF-α.

In conclusion, this study revealed a relationship between Ndr2 kinase, microglial responses, and the hyperglycemic environment, characteristic of diabetic retinopathy.

For future work, it would be intriguing to evaluate the expression and regulation of other inflammatory cytokines in Ndr2 downregulated or KO microglial cells, contributing to a more comprehensive understanding of the immune response. The assessment of ROS levels under hyperglycemic conditions would also be interesting to shed light on potential mechanisms linking oxidative stress to NDR2 kinase activity. Investigating the genetic and

epigenetic regulation of the Ndr2 gene in microglial cells exposed to high glucose levels holds promise for revealing regulatory elements that contribute to its expression and activity. Lastly, extending the study to an in vivo Ndr2 knockout mouse model would provide a more physiologically relevant setting to examine retinal microglial responses, validating findings from in vitro studies and offering a deeper insight into the repercussions of Ndr2 absence.

CHAPTER 6 – References

6.1 References:

[1] H. Kolb, "WEBVISION: The Organization of the Retina and Visual System," 2011. https://webvision.med.utah.edu/book/part-i-foundations/simple-anatomy-of-the-retina/.

[2] "How the Eyes Work | National Eye Institute." https://www.nei.nih.gov/learn-about-eye-health/healthy-vision/how-eyes-work (accessed Apr. 01, 2023).

[3] L. Semerád and M. Drahanský, "Retinal Vascular Characteristics," *Adv. Comput. Vis. Pattern Recognit.*, pp. 309–354, 2020, doi: 10.1007/978-3-030-27731-4_11.

[4] R. López-Elizalde *et al.*, "Anatomy of the optic nerve based on cadaveric dissections and its neurosurgical approaches: a comprehensive review," *Sechenov Med. J.*, vol. 12, no. 4, pp. 5–18, Nov. 2021, doi: 10.47093/2218-7332.2021.12.4.5-18.

[5] S. Yang, J. Zhou, and D. Li, "Functions and Diseases of the Retinal Pigment Epithelium," *Front. Pharmacol.*, vol. 12, p. 727870, Jul. 2021, doi: 10.3389/FPHAR.2021.727870/BIBTEX.

[6] T. W. Gardner, D. A. Antonetti, A. J. Barber, K. F. LaNoue, and S. W. Levison, "Diabetic retinopathy: More than meets the eye," *Surv. Ophthalmol.*, vol. 47, no. SUPPL. 2, pp. S253–S262, Dec. 2002, doi: 10.1016/S0039-6257(02)00387-9.

[7] Y. Sun and L. E. H. Smith, "Retinal Vasculature in Development and Diseases," *Annu. Rev. Vis. Sci.*, vol. 4, p. 101, Sep. 2018, doi: 10.1146/ANNUREV-VISION-091517-034018.

[8] N. Mahabadi and Y. Al Khalili, *Neuroanatomy, Retina*. StatPearls Publishing, 2022.

[9] J. Feher, "Vision," in *Quantitative Human Physiology*, Academic Press, 2012, pp. 386–400.

[10] M. Wilson and D. I. Vaney, "Amacrine Cells," in *The Senses: A Comprehensive Reference*, vol. 1, Academic Press, 2008, pp. 361–367.

[11] C. A. Chapot, T. Euler, and T. Schubert, "How do horizontal cells 'talk' to cone photoreceptors? Different levels of complexity at the cone–horizontal cell synapse," *J. Physiol.*, vol. 595, no. 16, p. 5495, Aug. 2017, doi: 10.1113/JP274177.

[12] B. Mead and S. Tomarev, "Evaluating Retinal Ganglion Cell Loss and Dysfunction," *Exp. Eye Res.*, vol. 151, p. 96, 2016, doi: 10.1016/J.EXER.2016.08.006.

[13] R. Nelson, "Visual Responses of Ganglion Cells," in *Webvision: The Organization of the*

Retina and Visual System, University of Utah Health Sciences Center, 2007.

[14] E. Vecino, F. D. Rodriguez, N. Ruzafa, X. Pereiro, and S. C. Sharma, "Glia–neuron interactions in the mammalian retina," *Prog. Retin. Eye Res.*, vol. 51, pp. 1–40, Mar. 2016, doi: 10.1016/J.PRETEYERES.2015.06.003.

[15] A. Reichenbach and A. Bringmann, "Glia of the human retina," *Glia*, vol. 68, no. 4, pp. 768–796, Apr. 2020, doi: 10.1002/GLIA.23727.

[16] K. O. Cohrt, "Macrophages and Microglia – Same but Different!," *tempobioscience*, 2018.

[17] F. Li, D. Jiang, and M. A. Samuel, "Microglia in the developing retina," *Neural Dev.*, vol. 14, no. 1, Dec. 2019, doi: 10.1186/S13064-019-0137-X.

[18] E. Murenu, M. J. Gerhardt, M. Biel, and S. Michalakis, "More than meets the eye: The role of microglia in healthy and diseased retina," *Front. Immunol.*, vol. 13, p. 1006897, Nov. 2022, doi: 10.3389/FIMMU.2022.1006897/BIBTEX.

[19] W. Y. Chan, S. Kohsaka, and P. Rezaie, "The origin and cell lineage of microglia: new concepts," *Brain Res. Rev.*, pp. 344–354, Feb. 2006, doi: 10.1016/J.BRAINRESREV.2006.11.002.

[20] K. Rashid, I. Akhtar-Schaefer, and T. Langmann, "Microglia in retinal degeneration," *Front. Immunol.*, vol. 10, no. AUG, p. 474669, Aug. 2019, doi: 10.3389/FIMMU.2019.01975/BIBTEX.

[21] A. Sapra and P. Bhandari, "Diabetes Mellitus," *StatPearls*, Jun. 2022, Accessed: Apr. 22, 2023. [Online]. Available: https://www.ncbi.nlm.nih.gov/books/NBK551501/.

[22] "International Diabetes Federation." https://www.idf.org/ (accessed Apr. 22, 2023).

[23] S. H. Sinclair, E. Miller, K. S. Talekar, and S. S. Schwartz, "Diabetes mellitus associated neurovascular lesions in the retina and brain: A review," *Front. Ophthalmol.*, vol. 2, p. 72, Oct. 2022, doi: 10.3389/FOPHT.2022.1012804.

[24] WHO, "Diabetic retinopathy screening: a short guide: increase effectiveness, maximize benefits and minimize harm." https://apps.who.int/iris/handle/10665/336660.

[25] L. Tang, G. T. Xu, and J. F. Zhang, "Inflammation in diabetic retinopathy: possible roles in pathogenesis and potential implications for therapy," *Neural Regen. Res.*, vol. 18, no. 5, pp. 976–982, May 2023, doi: 10.4103/1673-5374.355743.

[26] E. J. Duh, J. K. Sun, and A. W. Stitt, "Diabetic retinopathy: current understanding, mechanisms, and treatment strategies," *JCI insight*, vol. 2, no. 14, Jul. 2017, doi: 10.1172/JCI.INSIGHT.93751.

[27] R. Simó and C. Hernández, "Neurodegeneration in the diabetic eye: new insights and therapeutic perspectives," *Trends Endocrinol. Metab.*, vol. 25, no. 1, pp. 23–33, Jan. 2014, doi: 10.1016/J.TEM.2013.09.005.

[28] W. Wang and A. C. Y. Lo, "Diabetic Retinopathy: Pathophysiology and Treatments," *Int. J. Mol. Sci.*, vol. 19, no. 6, Jun. 2018, doi: 10.3390/IJMS19061816.

[29] R. A. Kowluru and P. S. Chan, "Oxidative stress and diabetic retinopathy," *Exp. Diabetes Res.*, vol. 2007, 2007, doi: 10.1155/2007/43603.

[30] J. Lechner, O. E. O'Leary, and A. W. Stitt, "The pathology associated with diabetic retinopathy," *Vision Res.*, vol. 139, pp. 7–14, Oct. 2017, doi: 10.1016/J.VISRES.2017.04.003.

[31] C. Altmann and M. H. H. Schmidt, "The Role of Microglia in Diabetic Retinopathy: Inflammation, Microvasculature Defects and Neurodegeneration," *Int. J. Mol. Sci.*, vol. 19, no. 1, Jan. 2018, doi: 10.3390/IJMS19010110.

[32] N. Demircan, B. G. Safran, M. Soylu, A. A. Ozcan, and S. Sizmaz, "Determination of vitreous interleukin-1 (IL-1) and tumour necrosis factor (TNF) levels in proliferative diabetic retinopathy," *Eye (Lond).*, vol. 20, no. 12, pp. 1366–1369, 2006, doi: 10.1038/SJ.EYE.6702138.

[33] S. Doganay *et al.*, "Comparison of serum NO, TNF-α, IL-1β, sIL-2R, IL-6 and IL-8 levels with grades of retinopathy in patients with diabetes mellitus," *Eye 2002 162*, vol. 16, no. 2, pp. 163–170, May 2002, doi: 10.1038/sj.eye.6700095.

[34] J. D. Boss *et al.*, "Assessment of Neurotrophins and Inflammatory Mediators in Vitreous of Patients With Diabetic Retinopathy," *Invest. Ophthalmol. Vis. Sci.*, vol. 58, no. 12, p. 5594, Oct. 2017, doi: 10.1167/IOVS.17-21973.

[35] A. Carmo, J. G. Cunha-Vaz, A. P. Carvalho, and M. C. Lopes, "l-Arginine transport in retinas from streptozotocin diabetic rats: correlation with the level of IL-1β and NO synthase activity," *Vision Res.*, vol. 39, no. 23, pp. 3817–3823, Nov. 1999, doi: 10.1016/S0042-6989(99)00117-0.

[36] F. I. Baptista, C. A. Aveleira, Á. F. Castilho, and A. F. Ambrósio, "Elevated Glucose and

Interleukin-1 β Differentially Affect Retinal Microglial Cell Proliferation," *Mediators Inflamm.*, vol. 2017, 2017, doi: 10.1155/2017/4316316.

[37] C. Harada *et al.*, "Role of monocyte chemotactic protein-1 and nuclear factor kappa B in the pathogenesis of proliferative diabetic retinopathy," *Diabetes Res. Clin. Pract.*, vol. 74, no. 3, pp. 249–256, Dec. 2006, doi: 10.1016/j.diabres.2006.04.017.

[38] R. A. Kowluru, P. Koppolu, S. Chakrabarti, and S. Chen, "Diabetes-induced activation of nuclear transcriptional factor in the retina, and its inhibition by antioxidants," *Free Radic. Res.*, vol. 37, no. 11, pp. 1169–1180, Nov. 2003, doi: 10.1080/10715760310001604189.

[39] U. M. Kinuthia, A. Wolf, and T. Langmann, "Microglia and Inflammatory Responses in Diabetic Retinopathy," *Front. Immunol.*, vol. 11, p. 564077, Nov. 2020, doi: 10.3389/FIMMU.2020.564077/BIBTEX.

[40] A. Hergovich, "The Roles of NDR Protein Kinases in Hippo Signalling," *Genes (Basel).*, vol. 7, no. 5, May 2016, doi: 10.3390/GENES7050021.

[41] P. F. Santos, B. Fazendeiro, F. C. Luca, A. F. Ambrósio, and H. Léger, "The NDR/LATS protein kinases in neurobiology: Key regulators of cell proliferation, differentiation and migration in the ocular and central nervous system," *Eur. J. Cell Biol.*, vol. 102, no. 2, p. 151333, Jun. 2023, doi: 10.1016/J.EJCB.2023.151333.

[42] A. Hergovich, M. R. Stegert, D. Schmitz, and B. A. Hemmings, "NDR kinases regulate essential cell processes from yeast to humans," *Nat. Rev. Mol. Cell Biol. 2006 74*, vol. 7, no. 4, pp. 253–264, Apr. 2006, doi: 10.1038/nrm1891.

[43] X. Ye, N. Ong, H. An, and Y. Zheng, "The Emerging Roles of NDR1/2 in Infection and Inflammation," *Front. Immunol.*, vol. 11, Mar. 2020, doi: 10.3389/FIMMU.2020.00534/PDF.

[44] H. Boubakri, "Recent progress in CRISPR/Cas9-based genome editing for enhancing plant disease resistance," *Gene*, vol. 866, p. 147334, May 2023, doi: 10.1016/J.GENE.2023.147334.

[45] J. A. Doudna and E. Charpentier, "Genome editing. The new frontier of genome engineering with CRISPR-Cas9," *Science*, vol. 346, no. 6213, Nov. 2014, doi: 10.1126/SCIENCE.1258096.

[46] M. A. Mengstie and B. Z. Wondimu, "Mechanism and Applications of CRISPR/Cas-9-

Mediated Genome Editing," *Biologics*, vol. 15, p. 353, 2021, doi: 10.2147/BTT.S326422.

[47] F. Jiang and J. A. Doudna, "CRISPR-Cas9 Structures and Mechanisms," *Annu. Rev. Biophys.*, vol. 46, pp. 505–529, May 2017, doi: 10.1146/ANNUREV-BIOPHYS-062215-010822.

[48] F. A. Ran, P. D. Hsu, J. Wright, V. Agarwala, D. A. Scott, and F. Zhang, "Genome engineering using the CRISPR-Cas9 system," *Nat. Protoc. 2013 811*, vol. 8, no. 11, pp. 2281–2308, Oct. 2013, doi: 10.1038/nprot.2013.143.

[49] Y. Mei, Y. Wang, H. Chen, Z. S. Sun, and X. Da Ju, "Recent Progress in CRISPR/Cas9 Technology," *J. Genet. Genomics*, vol. 43, no. 2, pp. 63–75, Feb. 2016, doi: 10.1016/J.JGG.2016.01.001.

[50] D. Collias and C. L. Beisel, "CRISPR technologies and the search for the PAM-free nuclease," *Nat. Commun. 2021 121*, vol. 12, no. 1, pp. 1–12, Jan. 2021, doi: 10.1038/s41467-020-20633-y.

[51] E. Janik, M. Niemcewicz, M. Ceremuga, L. Krzowski, J. Saluk-Bijak, and M. Bijak, "Various Aspects of a Gene Editing System—CRISPR–Cas9," *Int. J. Mol. Sci. 2020, Vol. 21, Page 9604*, vol. 21, no. 24, p. 9604, Dec. 2020, doi: 10.3390/IJMS21249604.

[52] E. Blasi, R. Barluzzi, V. Bocchini, R. Mazzolla, and F. Bistoni, "Immortalization of murine microglial cells by a v-raf/v-myc carrying retrovirus," *J. Neuroimmunol.*, vol. 27, no. 2–3, pp. 229–237, 1990, doi: 10.1016/0165-5728(90)90073-V.

[53] W. Russell and R. Burch, *The principles of humane experimental technique*. 1959.

[54] T. L. Riss *et al.*, "Cell Viability Assays," *Assay Guid. Man.*, Jul. 2016, Accessed: Apr. 07, 2023. [Online]. Available: https://www.ncbi.nlm.nih.gov/books/NBK144065/.

[55] M. Carter and J. Shieh, "Gene Delivery Strategies," *Guid. to Res. Tech. Neurosci.*, pp. 239–252, Jan. 2015, doi: 10.1016/B978-0-12-800511-8.00011-3.

[56] A. Fus-Kujawa *et al.*, "An Overview of Methods and Tools for Transfection of Eukaryotic Cells in vitro," *Front. Bioeng. Biotechnol.*, vol. 9, p. 701031, Jul. 2021, doi: 10.3389/FBIOE.2021.701031/BIBTEX.

[57] M. Vargas-Soria, M. García-Alloza, and M. Corraliza-Gómez, "Effects of diabetes on microglial physiology: a systematic review of in vitro, preclinical and clinical studies," *J. Neuroinflammation 2023 201*, vol. 20, no. 1, pp. 1–30, Mar. 2023, doi: 10.1186/S12974-023-02740-X.

[58] H. Léger, E. Santana, W. A. Beltran, and F. C. Luca, "Preparation of mouse retinal cryo-sections for immunohistochemistry," *J. Vis. Exp.*, vol. 2019, no. 149, pp. 1–6, 2019, doi: 10.3791/59683.

[59] X. Zhang, H. Dong, S. Zhang, S. Lu, J. Sun, and Y. Qian, "Enhancement of LPS-induced microglial inflammation response via TLR4 under high glucose conditions," *Cell. Physiol. Biochem.*, vol. 35, no. 4, pp. 1571–1581, Apr. 2015, doi: 10.1159/000373972.

[60] P. Kongtawelert, C. Kaewmool, T. Phitak, M. Phimphilai, P. Pothacharoen, and T. H. Shwe, "Sesamin protects against neurotoxicity via inhibition of microglial activation under high glucose circumstances through modulating p38 and JNK signaling pathways," *Sci. Rep.*, vol. 12, no. 1, p. 11296, Dec. 2022, doi: 10.1038/S41598-022-15411-3.

[61] C. F. Hsieh, C. K. Liu, C. T. Lee, L. E. Yu, and J. Y. Wang, "Acute glucose fluctuation impacts microglial activity, leading to inflammatory activation or self-degradation," *Sci. Reports 2019 91*, vol. 9, no. 1, pp. 1–16, Jan. 2019, doi: 10.1038/s41598-018-37215-0.

[62] A. R. Santiago, A. J. Cristóvão, P. F. Santos, C. M. Carvalho, and A. F. Ambrósio, "High glucose induces caspase-independent cell death in retinal neural cells," *Neurobiol. Dis.*, vol. 25, no. 3, pp. 464–472, Mar. 2007, doi: 10.1016/J.NBD.2006.10.023.

[63] K. Lv, H. Ying, G. Hu, J. Hu, Q. Jian, and F. Zhang, "Integrated multi-omics reveals the activated retinal microglia with intracellular metabolic reprogramming contributes to inflammation in STZ-induced early diabetic retinopathy," *Front. Immunol.*, vol. 13, Sep. 2022, doi: 10.3389/FIMMU.2022.942768/PDF.

[64] Q. Yin *et al.*, "Pharmacological Inhibition of Galectin-3 Ameliorates Diabetes-Associated Cognitive Impairment, Oxidative Stress and Neuroinflammation in vivo and in vitro," *J. Inflamm. Res.*, vol. 13, p. 533, 2020, doi: 10.2147/JIR.S273858.

[65] D. Lee and H. S. Hong, "Substance P Alleviates Retinal Pigment Epithelium Dysfunction Caused by High Glucose-Induced Stress," *Life*, vol. 13, no. 5, May 2023, doi: 10.3390/LIFE13051070.

[66] G. N. Costa, J. Vindeirinho, C. Cavadas, A. F. Ambrósio, and P. F. Santos, "Contribution of TNF receptor 1 to retinal neural cell death induced by elevated glucose," *Mol. Cell. Neurosci.*, vol. 50, no. 1, pp. 113–123, May 2012, doi: 10.1016/J.MCN.2012.04.003.

[67] A. A. D. Sharif and A. Hergovich, "The NDR/LATS protein kinases in immunology and cancer biology," *Semin. Cancer Biol.*, vol. 48, pp. 104–114, Feb. 2018, doi: 10.1016/J.SEMCANCER.2017.04.010.

[68] A. Enomoto, N. Kido, M. Ito, N. Takamatsu, and K. Miyagawa, "Serine-threonine kinase 38 is regulated by glycogen synthase kinase-3 and modulates oxidative stress-induced cell death," *Free Radic. Biol. Med.*, vol. 52, no. 2, pp. 507–515, Jan. 2012, doi: 10.1016/J.FREERADBIOMED.2011.11.006.

[69] J. Iannucci, H. V. Rao, and P. Grammas, "High Glucose and Hypoxia-Mediated Damage to Human Brain Microvessel Endothelial Cells Induces an Altered, Pro-Inflammatory Phenotype in BV-2 Microglia In Vitro," *Cell. Mol. Neurobiol.*, vol. 42, no. 4, p. 985, May 2022, doi: 10.1007/S10571-020-00987-Z.

[70] S. Mylvaganam, S. A. Freeman, and S. Grinstein, "The cytoskeleton in phagocytosis and macropinocytosis," *Curr. Biol.*, vol. 31, no. 10, pp. R619–R632, May 2021, doi: 10.1016/J.CUB.2021.01.036.

[71] O. Stork, A. Zhdanov, A. Kudersky, T. Yoshikawa, K. Obata, and H. C. Pape, "Neuronal Functions of the Novel Serine/Threonine Kinase Ndr2," *J. Biol. Chem.*, vol. 279, no. 44, pp. 45773–45781, Oct. 2004, doi: 10.1074/JBC.M403552200.

[72] W. Fan, W. Huang, J. Chen, N. Li, L. Mao, and S. Hou, "Retinal microglia: Functions and diseases," *Immunology*, vol. 166, no. 3, pp. 268–286, Jul. 2022, doi: 10.1111/IMM.13479.

[73] F. J. Shi *et al.*, "Is Iba-1 protein expression a sensitive marker for microglia activation in experimental diabetic retinopathy?," *Int. J. Ophthalmol.*, vol. 14, no. 2, p. 200, Feb. 2021, doi: 10.18240/IJO.2021.02.04.

[74] H. Léger *et al.*, "Ndr kinases regulate retinal interneuron proliferation and homeostasis," *Sci. Rep.*, vol. 8, no. 1, p. 12544, Dec. 2018, doi: 10.1038/S41598-018-30492-9.

[75] C. Zenobia and G. Hajishengallis, "Basic biology and role of interleukin-17 in immunity and inflammation," *Periodontol. 2000*, vol. 69, no. 1, p. 142, Oct. 2015, doi: 10.1111/PRD.12083.

[76] N. Parameswaran and S. Patial, "Tumor Necrosis Factor-α Signaling in Macrophages," *Crit. Rev. Eukaryot. Gene Expr.*, vol. 20, no. 2, p. 87, 2010, doi:

10.1615/CRITREVEUKARGENEEXPR.V20.I2.10.

[77] Y. Quan, C. T. Jiang, B. Xue, S. G. Zhu, and X. Wang, "High glucose stimulates TNFα and MCP-1 expression in rat microglia via ROS and NF-κB pathways," *Acta Pharmacol. Sin.*, vol. 32, no. 2, p. 188, Feb. 2011, doi: 10.1038/APS.2010.174.

[78] J. Song and J. E. Lee, "ASK1 modulates the expression of microRNA Let7A in microglia under high glucose in vitro condition," *Front. Cell. Neurosci.*, vol. 9, no. MAY, May 2015, doi: 10.3389/FNCEL.2015.00198.

[79] A. M. Joussen *et al.*, "Nonsteroidal anti-inflammatory drugs prevent early diabetic retinopathy via TNF-alpha suppression," *FASEB J.*, vol. 16, no. 3, pp. 438–440, 2002, doi: 10.1096/FJ.01-0707FJE.

[80] D. S *et al.*, "Comparison of serum NO, TNF-alpha, IL-1beta, sIL-2R, IL-6 and IL-8 levels with grades of retinopathy in patients with diabetes mellitus," *Eye (Lond).*, vol. 16, no. 2, pp. 163–170, Mar. 2002, doi: 10.1038/SJ.EYE.6700095.

[81] A. W. Qiu, Z. Bian, P. A. Mao, and Q. H. Liu, "IL-17A exacerbates diabetic retinopathy by impairing Müller cell function via Act1 signaling," *Exp. Mol. Med.*, vol. 48, no. 12, p. e280, Dec. 2016, doi: 10.1038/EMM.2016.117.

[82] Z. Liu *et al.*, "NDR2 promotes the antiviral immune response via facilitating TRIM25-mediated RIG-I activation in macrophages," *Sci. Adv.*, vol. 5, no. 2, Feb. 2019, doi: 10.1126/SCIADV.AAV0163/SUPPL_FILE/AAV0163_SM.PDF.

[83] H. Léger *et al.*, "Ndr kinases regulate retinal interneuron proliferation and homeostasis," *Sci. Rep.*, vol. 8, no. 1, Dec. 2018, doi: 10.1038/S41598-018-30492-9.